Cyclometalated Gold(III) Complexes Bearing DACH Ligands

Sailajah Gukathasan, Sean Parkin, and Samuel G. Awuah*

Department of Chemistry, University of Kentucky, Lexington, Kentucky 40506, United States

S *Supporting Information*

ABSTRACT: The synthesis of a novel class of cyclometalated gold(III) complexes supported by benzoylpyridine, benzylpyridine, and (1R,2R)-(+)-1,2-diaminocyclohexane (DACH) ligands, along with their crystal structures, is reported. These compounds provide a new scaffold to investigate biological properties of gold(III) complexes. The six complexes were prepared and characterized, following reactions of (C,N) cyclometalated gold(III) scaffolds, $[Au(C^\wedge N)Cl_2]$ with DACH, which yielded a new series of cyclometaled gold(III), **3−5**, of the type $[Au(C^\wedge NH)(DACH)_2]^+$ and the nitrogen-substituted cyclometalated Au(III), **6−8**, of the type $[Au(C^\wedge N)(DACH)]^{2+}$. Antiproliferative activity of these complexes in a panel of cancer cells showed promising results with IC_{50} in the micromolar range and selectivity over normal epithelial cells, MRC5. Whereas **8** shows minimal interaction with superhelical DNA except at high gold concentrations of 500 μM, complex **5** does not show interaction even at 1000 μM. The complexes display significant uptake in OVCAR8 cancer cells within 200−1200 pmol/million cells with the exception of complex **4**. Differential cellular uptake was observed for the complexes; for example, while **3** and **8** display significant uptake, **4** showed minimal uptake. The compounds proved to be stable under physiological conditions and were minimally affected by either glutathione or sodium ascorbate. Cell cycle studies reveal a G1 arrest induced by representative complexes. The results reveal that enhanced Au(III) stabilization promoted by combined cyclometalated and DACH ligands may offer ligand tuning insights for novel anticancer drug design.

INTRODUCTION

Metal-based drugs have been broadly applied in the treatment of diseases such as rheumatoid arthritis, diabetes, and cancer, and as an antimicrobial agent.[1] Platinum(II)-based drugs are the first line of therapy for various cancer types including testicular, ovarian, melanoma, colorectal, and non-small cell lung cancers.[2−5] Carboplatin and oxaliplatin are newer generation platinum(II) drugs with improved tolerance compared to cisplatin.[2] Despite the success of platinum agents, major drawbacks exist, including innate and acquired resistance, nausea, nephrotoxicity, and neurotoxicity.[6] Alternative approaches to mitigate side effects associated with platinum therapy include the development of Pt(IV) complexes and the use of other metals such as Ti, Fe, Co, Ru, Os, Ir, and Au.[7,8]

Organometallic gold(III) complexes have found wide applications in catalysis, material science, medicinal inorganic chemistry, and probe development.[9−14] Despite the wide utility of these compounds, they are often unstable, undergoing rapid reduction to Au(I) or Au(0) and can be synthetically challenging to make.[15−18] Diverse Au(III) compounds with unique structural scaffolds have the potential to resolve the challenges stated above in order to provide improved applicative outcomes. The choice of ligands is critical in tuning Au(III) complex properties. Cyclometalation is a well-known strong sigma donating carbon donor strategy to stabilize Au complexes.[19,20] This can increase the energy of

the gold(III) $5d\sigma^*$ ($5d_{x^2-y^2}$) orbital, thus potentiating excited-state characteristics.[21] Different classes of cyclometalation exist, including $[C^\wedge N]$, $[C^\wedge C]$, and $[C^\wedge P]$, which coordinate to Au in a bidentate fashion and lock the Au(III) complex in an often planar four-coordinate geometry.[22−35] Other classes have $(C^\wedge N^\wedge N)$ or $(C^\wedge N^\wedge C)$ pincer ligands to stabilize the gold(III) center.[19,36−47] These cyclometalation strategies are amenable to the coordination of biologically relevant or ancillary donor ligands for diversification and improved activity.[19,37,48] The stability imparted by these ligands enables efficient catalysis with increased turnover number (TON) and longevity of complexes in physiological medium for improved biological efficacy.

The (1R,2R)-(+)-1,2-diaminocyclohexane (DACH) ligand is featured in the FDA-approved platinum(II) complex, oxaliplatin, which displays a different spectrum of activity from cisplatin with no cross resistance.[49,50] In catalysis, DACH and its derivatives have been employed in the prominent Pd-catalyzed asymmetric allylic alkylation reaction for the construction of stereogenic centers and C−C, C−O, C−S, C−N bond formation.[51,52] Whereas the DACH ligand has gained traction, motivated by the outlined successes in the fields of catalysis and medicine, very few gold DACH compounds exist.[53−58] Synthesis of diverse gold DACH
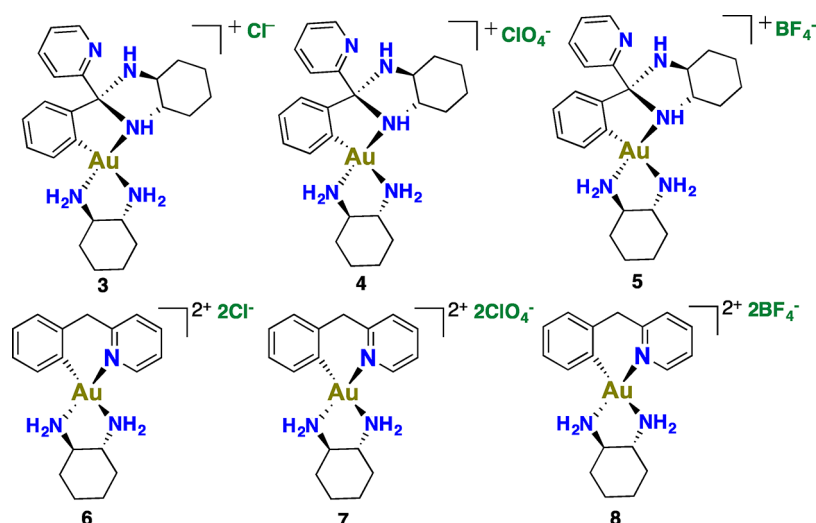
Figure 1. d^8-Cyclometalated Au(III) systems bearing DACH ligands.

Scheme 1. Synthetic Scheme To Access Cyclometalated (C^N) Gold(III) Complexes Bearing DACH Ligands
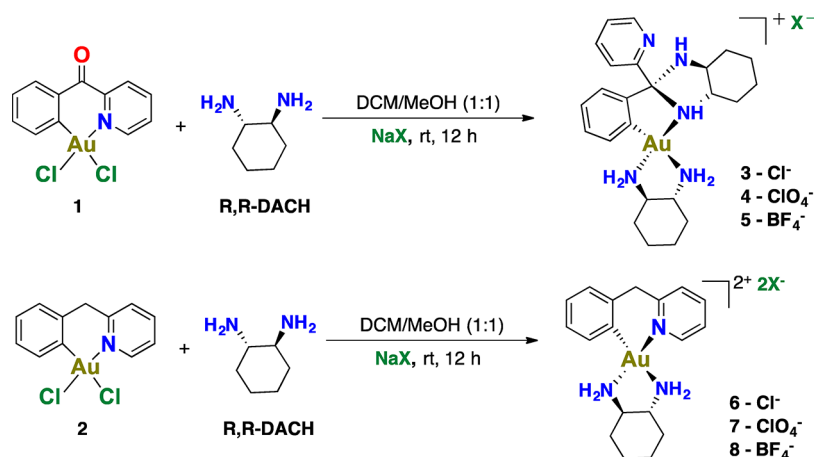
compounds can reveal structural insights that could lead to a new class of organogold reagents for useful applications. By combining the N-donor DACH ligand and the strong σ-donating character of C, N cyclometalated ligands, distinct gold(III) structure scaffolds can be obtained.

The antiproliferative effects of gold complexes have shown promise in preclinical studies.[7,59] Most gold(I) anticancer agents, including auranofin, target cysteine or selenocysteine-containing enzymes such as phosphatases, thioredoxin reductase, and cathepsins as their primary mode of action.[60,61] Gold(III) complexes supported by (C^N^N) or (C^N^C) pincer ligands on the other hand demonstrate a wide spectrum of activity.[36] Prominent targets of gold(III) anticancer agents include the ubiquitin-proteasome system, topoisomerase I, and autophagy.[62−64]

In this report, we describe the synthesis and characterization of novel cationic cyclometalated [C^N] gold(III) bearing DACH auxiliary ligands. When gold(III) supported by the benzoylpyridine ligand was used, a unique class of gold(III) complex was generated, with two DACH substitutions of the series [Au(C^NH)(DACH)$_2$]$^+$ (Figure 1). These complexes display high stability in complete Dulbecco's modified Eagle medium (DMEM) over 72 h and do not interact with plasmid DNA. To understand the biological activity of these complexes, we examined the antiproliferative profile against a panel of cancer cells. Furthermore, cellular uptake, cell cycle, and apoptosis of these complexes were investigated. The electrochemical behavior and DFT calculations of these compounds were studied. Knowledge of the fundamental properties of cyclometalated gold(III) bearing DACH ligands from this study unveils a new platform for the investigation of gold(III) compounds for potential utility across fields.

RESULTS AND DISCUSSION

Synthesis and Characterization. Cyclometalated gold-(III) starting materials were synthesized from commercially available benzoylpyridine and benzylpyridine ligands using reported methods. Coordination of the benzoylpyridine ligand to gold(III) ions was achieved by a reaction of the gold(III) trichloride complex bearing benzoylpyridine ligand in refluxing MeCN.[27] The reaction of benzylpyridine with HAuCl$_4$·3H$_2$O in refluxing water yielded the cyclometalated gold(III) supported by the benzylpyridine ligand.[27,29] At the onset, we rationalized that the structural difference in ligand systems could impart unique reactivity and stability upon diversification. Given the limited availability of chiral gold(III) complexes,[65,66] especially in biology, we sought to synthesize organometallic gold(III) complexes bearing chiral ligands for
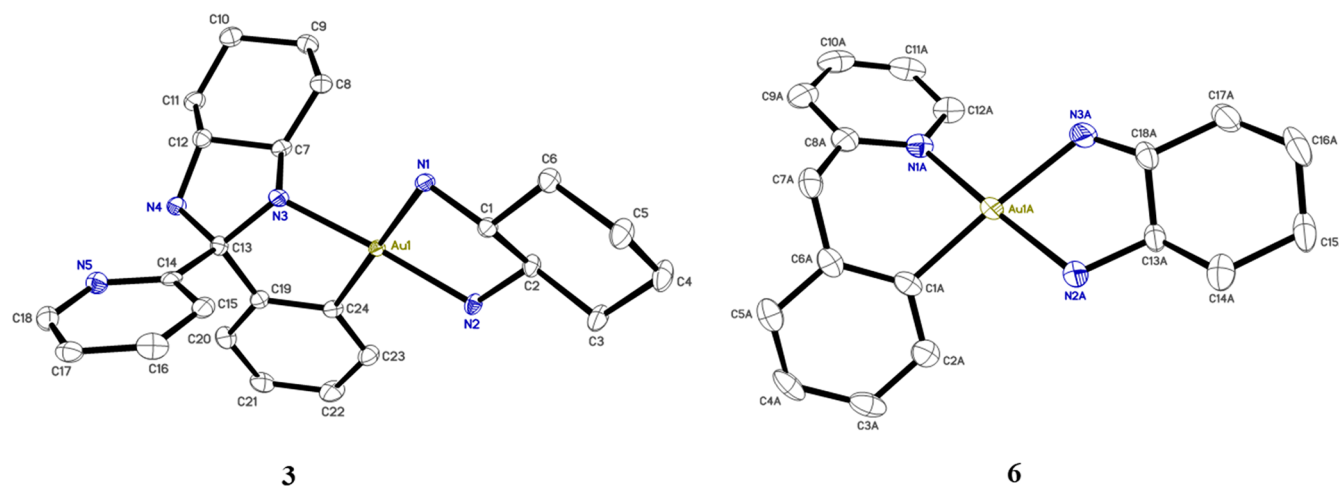
Figure 2. X-ray crystal structures of cations **3** and **6**, with ellipsoids drawn at 50%. Counterions, hydrogen atoms, minor components of disorder, and in **6**, a second copy of the cation, have been omitted to enhance clarity. The structure of **3** was refined with N1 and N2 both constrained as 50% NH and 50% NH2. This is supported by the requirement of modeling of anions Cl2 and Cl3 each at 50% due to their location on the crystallographic 2-fold axes of space group C2.

Table 1. Crystallographic Parameters for Complexes 3, 6, and 8

	3	6	8
formula	$C_{24}H_{34}AuClN_5$	$C_{18}H_{24}AuCl_2N_3$	$C_{18}H_{24}AuBClF_4N_3$
formula weight (M_r)	660.43	550.27	601.63
crystal system	monoclinic	monoclinic	orthorhombic
space group	C2	$P2_1$	$P2_12_12_1$
temperature (K)	90	90	90
a (Å)	20.8662(7)	7.8720(2)	11.2748(5)
b (Å)	10.4071(4)	24.9766(6)	17.8319(6)
c (Å)	13.4955(6)	10.8829(3)	23.1180(9)
α (deg)	90	90	90
β (deg)	120.3887(10)	98.984(1)	90
γ (deg)	90	90	90
volume (Å)	2528.01(17)	2113.50(9)	4647.9(3)
density (g/cm^3)	1.735	1.729	1.720
Z	4	4	8
μ (mm^{-1})	6.052	7.218	6.484
$F(000)$	1304.0	1064.0	2320.0
absorption correction	Multiscan	Multiscan	Multiscan
number of reflections	5794	9672	10677
T_{min}	0.334	0.552	0.575
T_{max}	0.430	0.746	0.785
R_{int}	0.0109	0.0165	0.0288
Refinement			
S	1.049	1.047	1.129
wR_2	0.0248	0.0389	0.0577
N_{par}	301	443	505

biological applications. Inspired by the use of DACH ligands in platinum-based (oxaliplatin) cancer therapy, our approach was to synthesize stable gold(III) complexes supported by auxiliary DACH donor ligands. These complexes are d^8 systems just like their FDA-approved Pt(II) counterparts.[2] Three gold(III) complexes, **3−5**, with DACH ligands were synthesized according to the procedure presented in Scheme 1. Respective (C,N) cyclometalated gold(III) was mixed with an equimolar amount of DACH ligand in DCM/MeOH (v/v = 1:1). We expected to obtain the monoligand-substituted product with DACH replacing the chloro ligands at the gold(III) center. However, we serendipitously discovered a rearrangement that provided a new cyclometalated complex type, [Au(C^NH)-

(DACH)$_2$]$^+$. A plausible mechanism is that nucleophilic attack of the electrophilic gold center displaces the chlorine trans to the aromatic carbon in **1**. This prompts bond breakage of the N(sp^2)−Au bond followed by the addition of a second DACH molecule to the gold and carbonyl, which breaks the C=O π bond. Protonation of the alcohol formed, and its elimination leads to the compound. The carbonyl group plays an important role in affecting the reactivity of the starting gold(III) complex, **1**, with the nucleophilic ancillary DACH ligands. In contrast, the expected ligand substituted complexes **6−8** of the type [Au(C^N)(DACH)]$^{2+}$ were accessible using the benzylpyridine supported (C, N) cyclometalated gold(III) compound, which does not contain the carbonyl functionality. The

reaction was carried out under room temperature conditions in DCM/MeOH using equimolar amounts of cyclometalated gold(III) and DACH ligands (Scheme 1).

The complexes were purified by recrystallization from methanol and fully characterized by ^{1}H NMR, ^{13}C{1H} NMR, ^{19}F NMR, mass spectrometry, high-performance liquid chromatography (HPLC), X-ray crystallography, and elemental analysis (Figures S1−S20). The complexes are moisture- and air-stable solids.

X-ray Crystallography. Single crystals of **3**, **6**, and **8** were grown by vapor diffusion of ether into a methanolic solution of concentrated gold complexes and analyzed by X-ray diffraction. The crystal structure of compound **3** revealed a unique rearrangement, which occurred during the reaction between benzoyl pyridine-supported cyclometalated gold(III) and (1R,2R)-(+)-1,2-DACH. The crystal structure shows formal coordination of one molecule of (1R,2R)-(+)-1,2-DACH to the gold(III) center, possibly, via ligand substitution. We further observed two C−N bonds formed between a second DACH molecule and the carbon formerly bearing the carbonyl group. A dangling pyridine ring, indicative of N(sp^2)−Au bond cleavage, is also observed in the structure. The X-ray structure of **3** reveals a Cs-symmetric distorted square-planar geometry around the gold center, with two amino groups from one DACH ligand, one amino group from a second DACH ligand, and one cyclometalation bond from the benzoyl pyridine ligand defining the d^8 Au(III) geometry as shown in Figure 2. The Au−C bond distance in the gold-benzoyl pyridine of 2.012(3) Å is relatively shorter than several cyclometalated gold compounds reported. Additionally, the Au−N bonds in the gold DACH ligands of 2.026(2) Å, 2.044(3) Å, and 2.126(3) Å, respectively, have short bonds, similar to Au−C bonds. These short bond distances are suggestive of strong bonding energy between the high-oxidation Au(III) and its DACH ligand. Consistent with our hypothesis, ligand tuning, herein, combining cyclometalation and DACH donor ligands, stabilized this high-oxidation state Au(III) complex. Similarly, the dicationic complex, **6**, has a Au−C bond distance of 2.031(5) Å between the gold and benzyl pyridine. The Au−N bond distances between gold and the DACH ligand were 2.031(4) Å, 2.048(3) Å, and 2.109(5) Å, respectively. The short bond lengths impart strong bonding energy in the high oxidation state Au(III) complex. The change in counterion from Cl$^-$ (**6**) to BF$_4^-$ (**8**) did not significantly affect geometry or bond distances of complexes, as shown in Table 3. However, major differences in crystal packing were realized, complex **3** being monoclinic and **6** being orthorhombic.

Solution Studies. We evaluated the spectrophotometric properties of these complexes in biologically relevant medium. In addition to assessing the spectrophotometric characteristics of the complexes, the use of DMEM, which contains several biological nucleophiles and reducing agents such as amino acids in high concentrations (mM), was used to study the stability of these complexes. We used UV−vis spectroscopy to investigate representative complexes **3** and **6**. The UV−vis spectrum of **3** displayed lower energy transitions between 560−575 nm and high energy transitions at 250 nm. We recorded the UV−vis spectra of benzoylpyridine and benzylpyridine ligands in the same conditions as complexes **3** and **6** to aid band assignment (Figures S33 and S34). These spectra indicated that the strong absorption band at ∼250 nm is due to intraligand transition in both complexes **3** and **6**. The longer wavelength absorption bands at 275, 350, and 575 nm

Table 2. Selected Interatomic Distances (Å) and Angles (deg) from the Crystal Structure (Complex 3) shown in Figure 2

	3
Au1−C24	2.012(3)
Au1−N2	2.026(2)
Au1−N3	2.044(3)
Au1−N1	2.126(3)
N1−C1	1.486(4)
N2−C2	1.497(4)
N3−C13	1.523(4)
N4−C13	1.469(4)
C13−C14	1.538(4)
C24−Au1−N2	96.51(12)
C24−Au1−N3	81.60(14)
N2−Au1−N3	176.90(11)
C24−Au1−N1	175.74(12)
N2−Au1−N1	82.86(11)
N3−Au1−N1	98.84(10)
C1−N1−Au1	106.54(18)
C2−N2−Au1	110.24(19)
C7−N3−Au1	116.45(19)
C13−N3−Au1	111.68(19)
N1−C1−C2	106.7(2)
N2−C2−C1	108.3(2)
N4−C13−N3	105.2(2)
N4−C13−C14	113.0(2)
C19−C13−C14	109.3(2)
N4−C13−C19	111.7(3)

Table 3. Selected Interatomic Distances (Å) and Angles (deg) from the Crystal Structure (Complexes 6 and 8) Shown in Figure 2

	6	8
Au1−N1	2.031(4)	2.042(6)
Au1−C1	2.031(5)	2.024(8)
Au1−N2	2.048(4)	2.018(6)
Au1−N3	2.109(5)	2.122(6)
N1−Au1−C1	88.7(2)	87.7(3)
N1−Au1−N2	176.57(19)	178.9(3)
C1−Au1−N2	93.9(2)	91.9(3)
N1−Au1−N3	94.72(18)	97.3(2)
C1−Au1−N3	176.5(2)	174.3(3)
N2−Au1−N3	82.65(18)	83.1(2)

most likely correspond to variations of metal-to-ligand or ligand-to-metal transitions related to the gold(III) center. The spectrophotometric phenomenon observed for **3** is similar to **6** only with minor spectral shifts. The characteristic UV−vis spectra of both **3** and **6** were minimally affected after 72 h in DMEM solution (Figures 3 and S25), indicative of the stability of these complexes in DMEM. This is important as it ensures that the potential anticancer agents do not decompose prematurely in the biologically relevant medium. Additionally, no precipitation was observed when the stock solutions of complexes **3** or **6** were diluted with aqueous DMEM. We did not observe any color change of both DMEM solutions of complexes **3** and **6** over a 72 h period. This is indicative of the lack of unwanted precipitation and potential reduction to elemental gold, which often shows a brown to golden coloration of the solution and its vial. Taken together, the
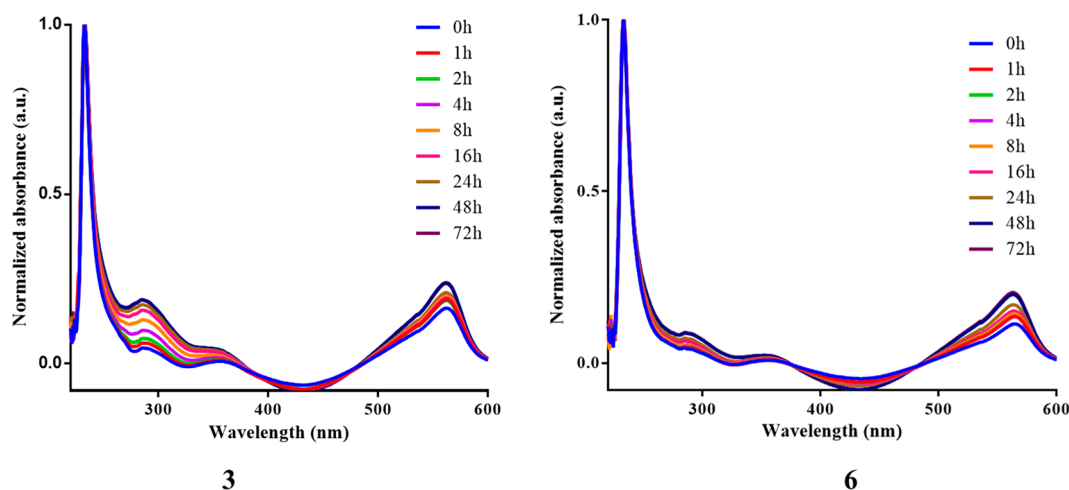
Figure 3. UV−vis spectrum of **3** (50 μM) and **6** (50 μM) in DMEM over a period of 72 h.

Table 4. IC$_{50}$ Values for Complexes 3−8 in a Panel of Cancerous and Normal Cell Lines

cell line	IC$_{50}$ (μM)							
	3	**4**	**5**	**6**	**7**	**8**	auranofin	cisplatin
OVCAR8	6.3 ± 0.04	1.2 ± 0.06	4.4 ± 0.07	14.8 ± 0.09	14.8 ± 0.06	14.8 ± 0.1	1.4 ± 0.03	2.8 ± 0.04
A2780	3.7 ± 0.1	3.7 ± 0.08	2.7 ± 0.03	1.3 ± 0.04	15.0 ± 0.22	5.6 ± 0.18	3.0 ± 0.03	2.0 ± 0.04
MCF7	5.0 ± 0.01	13.2 ± 0.01	5.2 ± 0.01	1.8 ± 0.01	1.5 ± 0.01	4.5 ± 0.02	1.1 ± 0.02	1.5 ± 0.01
RPE MYC	9.5 ± 0.02	9.5 ± 0.02	9.1 ± 0.03	14.4 ± 0.02	3.2 ± 0.03	1.7 ± 0.04	2.6 ± 0.01	3.8 ± 0.03
MRC5	>100.0	>100.0	>100.0	>100.0	>100.0	>100.0	>50.0	>50.0

new gold(III)-DACH complexes show significant stability in culture medium, necessary for further biological evaluation.

Reaction with Glutathione or Ascorbate. The reactivity of gold complexes with proteins has been well-documented,[67−73] unlike platinum agents, which have DNA as their primary target. Third-row transition metal complexes often act as π-Lewis acid centers with reactivity to soft bases and nucleophiles. Several biological nucleophiles react with transition-metal based anticancer complexes based on the electrophilicity, redox properties, and kinetic lability as the pathway to cytotoxic effects. In some cases, reactivity of biological reducing agents with transition-metal complexes deactivates complexes or initiates off-target effects. It is estimated that the tripeptide L-glutathione is ∼10 mM in cells,[37,74] and therefore, metal complexes need to bypass reduction to reach their target. To this end, we evaluated the reactivity of our gold(III)-DACH complexes with L-glutathione. The investigation proceeded with **5**, which has the scaffold of the type [Au(C^NH)(DACH)$_2$]$^+$ and **8** with the scaffold [Au(C^N)(DACH)]$^{2+}$ with the same tetrafluoroborate anion. These representative candidates were treated with the model biomolecule L-glutathione at a concentration of 50 mM in a 1:10 ratio and monitored over a time period of 12 or 24 h. We used ^{1}H NMR or UV−vis spectroscopic methods to monitor the reaction. When **5** was treated with GSH in DMSO-d_6, we did not observe any shift in resonance (multiplet, 2.75 ppm) corresponding to the methylene protons adjacent to the thiol group in GSH, which is consistent with reduced L-glutathione (Figure S27). The 7.4 ppm resonance (multiplet) of **5** started to split at 4 h with no further changes post 4 h to the 12 h window. Notably, the peaks did not increase in height or area throughout the course of the reaction. On treating **8** with GSH under similar conditions as **5**, immediate splitting and shifting of the 2.75 ppm resonance

were not observed (Figure S28). We did not observe changes in NMR resonances or a change in color of the reaction solutions, suggesting that these complexes are not reduced to elemental gold by GSH. Next, the reaction of gold(III)-DACH compounds was monitored by UV−vis spectroscopy to follow potential spectral changes of absorption bands associated with gold(III) in response to GSH (Figures S29−S30). Upon treatment of **5** with GSH, there was an increase in the strong absorption peak at 575 nm, corresponding to metal-to-ligand charge transition (MLCT) or ligand-to-metal charge transfer (LMCT). This change persisted over the 24 h time-course of the experiment. Moreover, **8** revealed similar changes in the peak at 575 nm. The results demonstrate minimal reactivity to L-glutathione in comparison to other gold(III) complexes, such as gold(III) dithiocarbamates,[75,76] which show rapid reduction upon treatment with GSH. The compounds described in this report have stability toward GSH as seen from the NMR and UV studies with the features of the starting gold(III) still present after 12 or 24 h. We further investigated the effect of another natural reducing agent, ascorbate, on the gold(III)-DACH complexes. We used sodium ascorbate, which has two peaks 245 and 285 nm in its UV absorption profile in DMEM (Figures S31 and S32). Over the 24 h time period for which the reaction of **5** or **8** with excess sodium ascorbate (1:20) was monitored, we observed significant peak increments in the two absorption bands for **5** and unaltered peaks for **8**. It is evident that **8** is highly stable toward sodium ascorbate reduction, while **5** is not over 24 h. We did not see any color change in the solution or precipitate formation while scanning the UV−vis spectrum of complexes **5** and **8** with ascorbate. In summary, the structural diversity as depicted in **5** and **8** has implications on the reactivity of the gold(III)-DACH compounds to biological reducing agents.
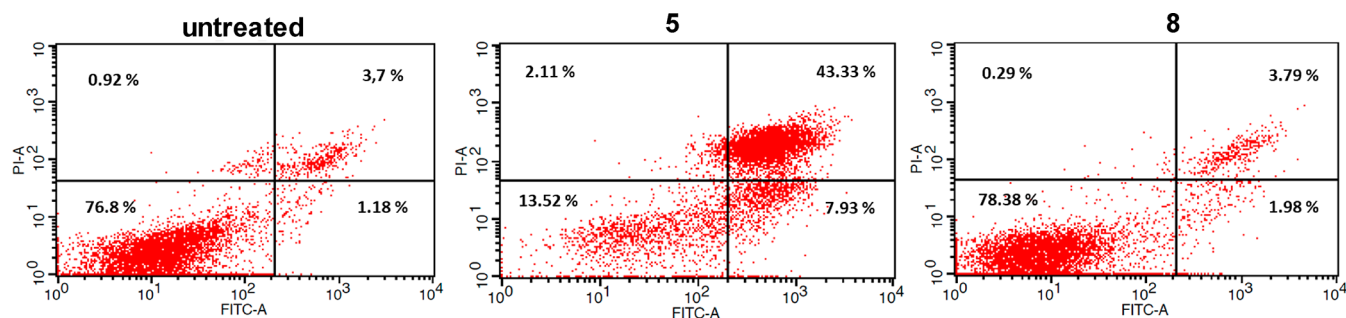
Figure 4. Apoptosis analysis (annexin V-FITC and propidium iodide assay) plot for complexes **5** and **8** (10 μM) in the OVCAR8 cell line.
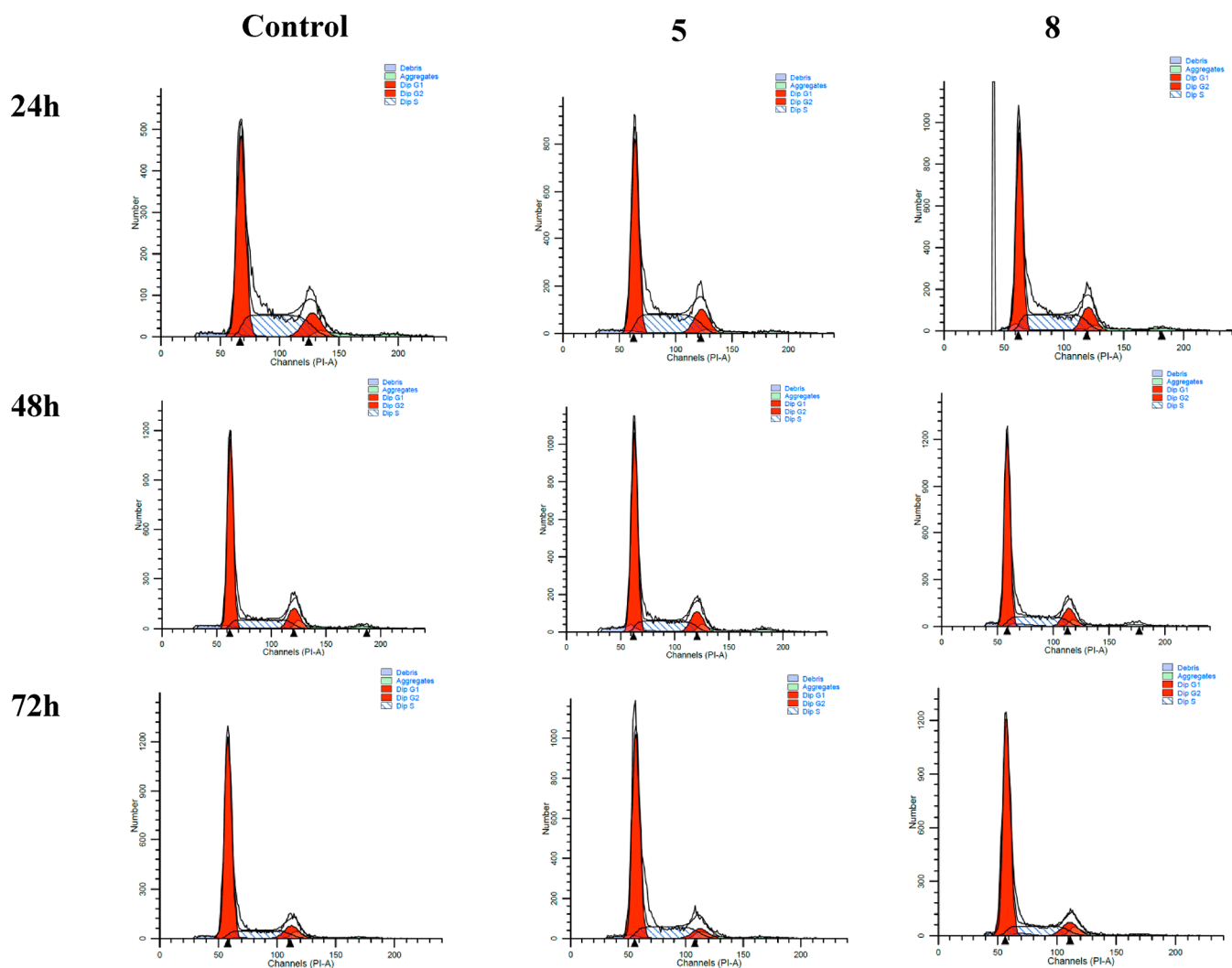
Figure 5. Histogram representing the different phases of the cell cycle of OVCAR8 in the presence or absence of complexes **5** and **8** (5 μM) over the course of 72 h. Twenty-four hour treated with **5**: G1:51.85%, S: 35.37%, G2/M: 12.78%, 48 h treated with **5**: G1:61.08%, S: 26.26%, G2/M: 12.66%, 72 h treated with **5**: G1:68.30%, S: 25.15%, G2/M: 6.55%, 24 h treated with **8**: G1:52.30%, S: 35.09%, G2/M: 12.61% 48 h treated with **8**: G1:62.47%, S: 25.45%, G2/M: 12.08%, 72 h treated with **8**: G1:70.93%, S: 20.38%, G2/M: 8.70%.

Antiproliferative Activity in Vitro. The antiproliferative properties of the gold(III) complexes **3−8**, cisplatin, and auranofin were evaluated by monitoring cellular growth inhibition using a crystal violet assay (see Experimental Section). The cytotoxic activity of the compounds was determined in a panel of human cancer cell lines including human ovarian carcinoma cell lines (OVCAR-8), human ovarian adenocarcinoma cell lines (A2780), Michigan Cancer Foundation-7 (MCF7- breast cancer cell lines), and human

retinal pigment epithelial cells engineered to overexpress MYC (RPE MYC). The concentration required to kill 50% of cells was extrapolated from dose−response curves, and these results have been summarized in Table 4 and Figure S21−S24. Generally, the complexes under investigation displayed moderate cytotoxicity in comparison to auranofin or cisplatin. Complexes **3−5** were more potent toward OVCAR8 and A2780 cell lines, which are of ovarian origin, whereas complexes **6−8** were more potent toward MCF7 and RPE

MYC cells, which are both c-MYC dependent for tumor growth. Complexes **6−8** were considerably more cytotoxic than auranofin and cisplatin in the c-MYC-dependent breast cancer, MCF7 cell line. In order to assess the compounds' selectivity for cancerous cells with respect to normal cell lines, they were also screened in normal lung fibroblasts (MRC5) as a representative model for noncancerous cells. The IC$_{50}$ values of **3−8** in the MRC5 cell line was approximately 100 μM. On the basis of the data, auranofin and cisplatin were more cytotoxic than these complexes in MRC5 cells. Together, the differential cytotoxicity observed in the varied cancer cells is a sound premise for structural diversity toward cancer cell selective gold-based drugs.

Apoptosis Studies. Following the cell viability study, we sought to understand the mechanism by which the complexes induced cell death. Widely accepted anticancer agents effect activity via apoptosis. The effect of the new gold(III) complexes on cells was examined by assessing the apoptotic pathway. Generally, apoptosis cells undergo morphological changes that lead to cell membrane disorientation. This can be detected by annexin V, and thus using annexin V-FITC/PI[77] in a dual staining fluorescence assisted cell sorting (FACS) analysis is useful. The experiment relies on the ability of fluorescent-labeled annexin V to bind phosphatidylserine on the outer leaflet of the plasma membrane when cells undergo apoptosis and a fluorescent DNA-intercalating dye, propidium iodide (PI), used to stain cells and detect dead cells. When untreated or treated cells are stained with these staining reagents, different populations of cells can be analyzed by flow cytometry depending on their forward and side scattering as well as the intensity corresponding to annexin V or PI. The cell populations are gated using appropriate controls, and the subpopulations are categorized into respective quadrants. Each quadrant of the apoptosis plot as displayed in Figure 4 can be described as (i) lower left quadrant, which is a population of live cells, demonstrating annexin V-FITC negative and PI negative cells; (ii) lower right quadrant, which is a population of early apoptotic cells, displaying annexin V-FITC positive and PI negative cells; (iii) upper right quadrant, which is a population of late apoptotic cells, that display annexin V-FITC positive and PI positive cells; and (iv) upper left quadrant, which is a population of nonviable necrotic cells that show annexin V- FITC negative and PI positive cells. Applying this approach, we treated OVCAR8 cells with complexes **5** and **8** (10 μM) for 48 h and analyzed the cells by using FACS. Complex **5** induced a large population of cells to undergo late-stage apoptosis, while complex **8** had the highest population of live cells. Experimental data proved that both complexes largely induced apoptosis and not necrosis (Figure 4 and Figure S26). We used auranofin and cisplatin as controls. The result is quite consistent with our cell viability study, which demonstrates particular effectiveness of **5** in OVCAR8 cells (Table 4).

Cell Cycle Studies. Anticancer agents often interfere with different phases of the cell cycle, and thus the nature of the cell cycle can be a useful tool to identify the mechanism of action of the complex.[78] We therefore analyzed the interference of complexes **5** and **8** with the different phases of the cell cycle using OVCAR8 cells (Figure 5). These complexes represent the two different classes of cyclometalated-DACH compounds described in this report. Both complexes **5** and **8** had high cell populations (~52.0%) in the G1 phase after 24 h following drug candidate treatment. After 48 h, both complexes induced G1 phase arrest, **5** had 61.0% of cells in G1 phase, and **8** had

62.5% cells in the G1 phase. The same pattern continued after 72 h treatment. Clearly, cell arrest happened at the G1 phase for both complexes **5** and **8**. In comparison, cisplatin is a well-known DNA cross-linker, which stalls the cell cycle at the S phase after 48 h and G2/M after 72 h. Consistent with DNA interaction studies of **5** and **8**, vide infra, the cell cycle result confirms that the DNA may not be the potential target of these compounds. Furthermore, auranofin is known to stall the cell cycle at the G1 phase,[78] displaying similarity with our gold complexes.

Cellular Uptake. We performed cellular uptake studies to evaluate the extent of intracellular accumulation of these cationic complexes. Cellular uptake of compounds often contributes to in vitro and in vivo anticancer activity, since most of the anticancer drug targets are intracellular.[78] In this experiment, OVCAR8 cells were treated with 10 μM of the gold drug candidates, **3−8**, or auranofin for 15 h. The cells were subsequently washed, digested with 500 μL concentrated HCl, and diluted to 5.0 mL using DI water and assayed using inductively coupled plasma optical emission spectroscopy (ICP-OES). Cellular uptake of complex **3** (400 pmol/million cell) and **8** (700 pmol/million cell) were relatively higher than complexes **4**, **5**, **6**, and **7** as seen in Figure 6. However, complex
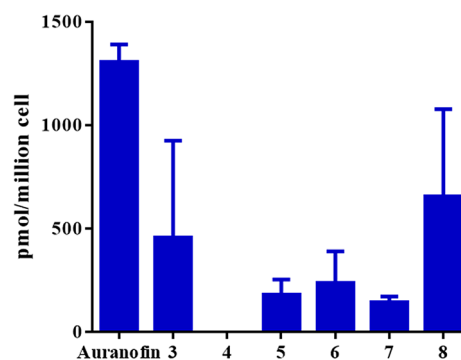
Figure 6. Cellular uptake of complexes **3−8** (10 μM) and auranofin in OVCAR8 cells after 15 h of incubation.

4 exhibited a cellular uptake lower than the detection limit under the same conditions. In general, complexes with the perchlorate anion, that is, **4** and **7**, displayed a lower uptake. In contrast, the neutral auranofin was taken up by approximately 2-fold more than **3** and **8**, which had a high cellular uptake among the gold(III)-DACH compounds investigated in this report. We can draw insights from the anion effect as the culprit for the differences observed in the cellular uptake profile of the complexes. First, the chloride counterion in **3** and **6** is relatively small in size, and hence the cationic character of the overall complex dictates the extent of uptake. The monocation, **3**, may possess an advantage over the dication, **6**, in crossing the plasma membrane due to reduced repulsion, which may likely explain the difference in uptake of complexes **3** and **6** bearing chloride anions. Second, with respect to **4** and **7**, the perchlorate anions are relatively large and possess the ability to induce ion-dipole interactions with the aqueous culture medium, which limits their ability to cross the lipophilic cell membrane. On the other hand, complexes with BF_4 anions showed very different uptake levels with no clear correlations to confidently support the observation. Our findings reveal that for these organogold(III)-DACH compounds, the choice of anion used can influence complex uptake

in cells. Overall, the compounds demonstrate relatively low intracellular accumulation, and this could be attributed to their cationic character as well as inherent anionic effects. Conceivably, the low uptake may contribute to the relatively moderate cytotoxic effect in cancerous cell lines.

Interactions with DNA. Previous studies proved that gold(III) complexes interact with protein and not DNA to cause cell death.[79] We therefore investigated the interaction of **5** (Figure 7, top) and **8** (Figure 7, bottom) with pUC19
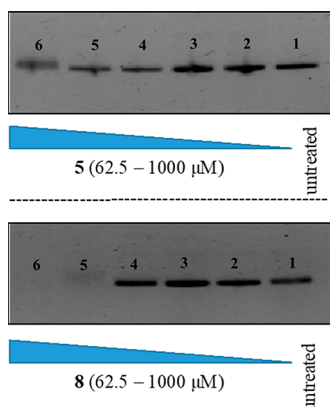
Figure 7. Agarose gel electrophoresis of pUC19 DNA treated with different concentration of complexes **5** (top) and **8** (bottom) after incubation of 24 h at 37 °C. Lane 1: DNA only; lanes 2−6: DNA + 62.5, 125, 250, 500, and 1000 μM of **5** or **8**.

plasmid DNA using agarose gel electrophoresis. As the concentration of complex **5** increased, the supercoiled plasmid DNA remained unaltered to about 1000 μM concentration, where visible smearing of the supercoiled form was observed. In slight contrast, when compound **8** was used, there was no significant change to the supercoiled form of DNA at concentrations <250 μM; however, at 500 μM and 1000 μM the bands in the gel smear and disappear, respectively. The gel images clearly indicate that both complexes **5** and **8** do not induce conformational changes or degradation of circular DNA at concentrations <250 μM. Overall, structural distinctions between **5** and **8** are responsible for the varied effects on DNA. It is possible that the distorted scaffold of **5** coupled with its enhanced stability attributed to relatively shorter Au−N bonds prevent DNA intercalation or kinetic lability for covalent binding to the nucleophilic portions of DNA such as guanine or adenine. Understandably, the degree of square-planar distortion adjudged from the crystal structure of **6** is smaller than in **5**, and thus an increased possibility for intercalation exists. In general, the two classes of gold(III) compounds display minimal interaction with DNA, which differentiates them from platinum agents in the clinic.[45,53,71]

Electrochemistry. The electrochemical behavior of the gold(III) complexes of the type [Au(C^NH)(DACH)$_2$]$^+$ and [Au(C^N)(DACH)]$^{2+}$ were characterized by cyclic voltammetry in anhydrous DMSO with 0.1 M NBu$_4$PF$_6$ as the supporting electrolyte. The electrochemical data of the complexes (**3**, **5**, **6**, **8**) investigated including starting reagents (**1**, **2**, DACH) are summarized in Table 5, and representative voltammograms are shown in Figure 8. The voltammograms of complexes **1**, **2**, **3**, **5**, **6**, **8**, and the DACH ligand in anhydrous DMSO solution with 0.10 M NBu$_4$PF$_6$ electrolyte were also conducted. The condition used was a scan rate of 100 mV/s, referenced to Ag/AgCl based on the position of the Fc/Fc+

Table 5. Reduction Potentials of Complexes 1, 2, 3, 5, 6, and 8

complex	reduction potential (V)				oxidation potential (V)
	E, (A)	$E_{1/2}$, (B/D)	E, Au(III)/Au(I)(C)	E, ligand centered	E, (E)
1	−0.58			−1.93	0.66
2		−0.88	−1.52		0.63
3	−0.70	−0.95	−1.40		0.68
5	−0.75	−0.95	−1.41		0.68
6		−0.86	−1.50		0.76
8		−0.86	−1.50		0.75

couple as an internal standard. The results are displayed in the Supporting Information, Figures S35−S41.

Complexes **3** and **5** displayed the same features in their cyclic voltammograms: An irreversible reduction (A) [**3** = −0.70 V; **5** = 0.75 V], quasi-reversible reduction/oxidation (B/D) [**3** = −0.95 V; **5** = −0.95 V], an irreversible reduction (C) [**3** = −1.40 V; **5** = 1.41], and oxidation (E) [**3** = +0.68; **5** = +0.68]. We assign the irreversible reduction event (A) to the ligand-centered reduction of benzoylpyridine. Quasi-reversible reduction/oxidation waves (B/D) are attributed to ligand−metal electron transfer based on the voltammograms of the starting gold(III) complexes, **1** and **2** (Table 5). The irreversible reduction (C) corresponds to Au(III)/Au(I) reduction, consistent with reported reduction potentials in the range of −0.95 to −1.50 V.[80] Moreover, the oxidation event (E) may likely be a ligand centered activity. Cyclic voltammograms of complexes **6** and **8** displayed slightly different features from complexes **3** and **5**. There was a prominent irreversible reduction event (A) corresponding to an event from the benzoylpyridine ligand, which is absent in the cyclic voltammograms of complexes **6** and **8**, while maintaining the other events (B/D) [**6** = −0.86 V; **8** = −0.86 V], (C) [**6** = −1.50 V; **8** = −1.50 V], and (E) [**6** = +0.76 V; **8** = +0.76 V] (Table 5).

Complexes **3** and **5** were prepared using **1** and the DACH ligand, while complexes **6** and **8** were prepared using **2** and the DACH ligand. It is worth noting that the diverse structural scaffolds significantly influence the electrochemical behavior. Furthermore, we performed electrochemical analysis of complexes **1**, **2**, or the DACH ligand alone (Figures S33−S39). Complex **1** exhibited two quasi-reversible events that correspond to (A/H) and (F/G) and an oxidation event (E) as shown in Figure S35. Complex **2** exhibited a quasi-reversible reduction/oxidation (B/D) and a reduction (C) attributed to Au(III)/Au(I) couple and an oxidation wave (E) as shown in Figure S36. There were no significant electrochemical events in the DACH ligand (Figure S37). Complexes **3** and **5** showed an irreversible reduction potential at −0.70 V and −0.75 V vs Ag/AgCl respectively (Table 5). This reduction potential is related to ligand centered reduction of benzoylpyridine. The ligand centered reduction in **1** was at −0.58 V vs Ag/AgCl. The formation of the rearranged complexes **3** and **5** from the reaction of **1** and DACH ligand destabilizes the ligand-centered reduction potential by 0.17 V (more negative) versus Ag/AgCl. This observation is a confirmation of rearrangement of complexes **3** and **5** with the substitution of the carbonyl group in the benzoylpyridine ligand. The starting material **1** displayed a reversible reduction potential at −1.93 V vs Ag/AgCl, which we attribute to ligand-based events from the
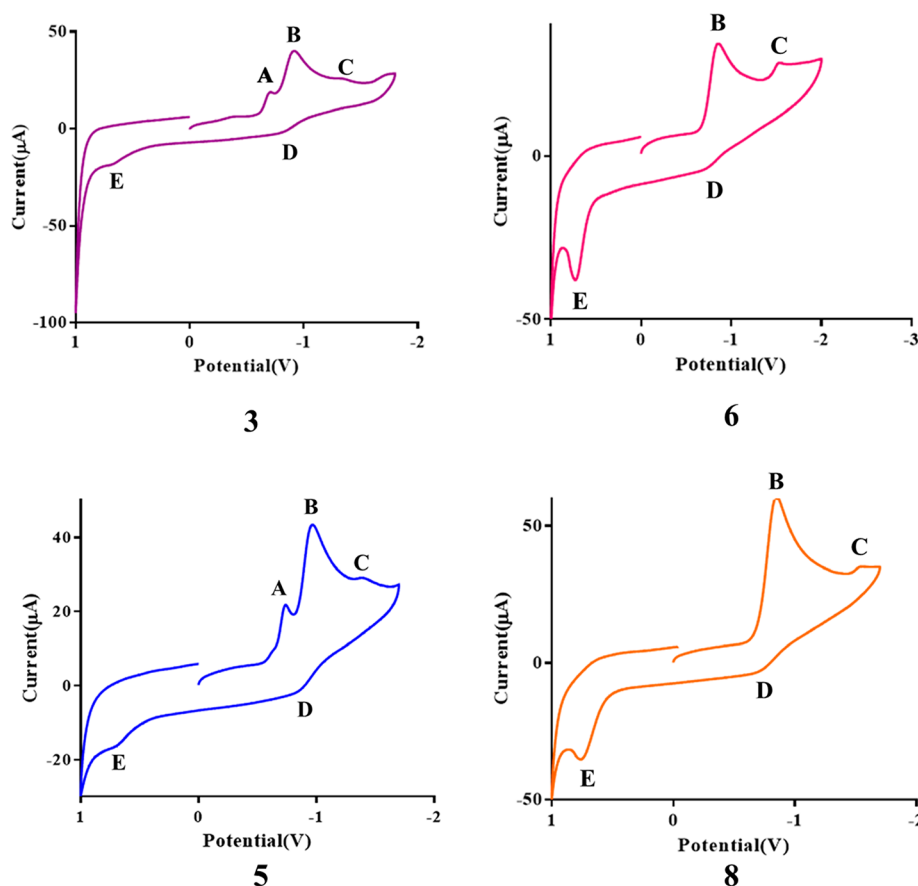
Figure 8. Cyclic voltammograms of complexes **3**, **5**, **6**, and **8**. This experiment was performed at room temperature in anhydrous DMSO solution with 0.10 M NBu$_4$PF$_6$ electrolyte at a scan rate of 100 mV/s. The potential is referenced to Ag/AgCl based on the position of the Fc/Fc+ couple as an internal standard.

benzoylpyridine. In all the electrochemical studies, we did not observe any shiny brown coloration indicative of metallic Au(0). Thus, we ruled out the possibility of Au(I)/Au(0) couple in all studied compounds. In addition, complexes **3** and **5** exhibited reduction potentials at −0.95 V and −1.41 V vs Ag/AgCl corresponding to ligand-centered and Au(III)/Au(I) reductions, respectively. All complexes **1**, **3**, and **5** displayed the same oxidation event Au(III)/Au(I)) at 0.68 V vs Ag/AgCl. The absence of Au(I)/Au(0) reduction in complexes **3** and **5** confirms the role of the DACH ligand to increase the stability of the Au(III) center. It is noteworthy that **3** and **5** had the same observed cyclic voltammogram regardless of the counterion present (Cl⁻ and BF$_4$⁻).

Moreover, complexes **6** and **8** displayed a quasi-reversible reduction potential (B/D) at −0.86 V vs Ag/AgCl and an irreversible reduction potential at (C) −1.5 V vs Ag/AgCl, which is related to the Au(III)/Au(I) couple. The starting material for these complexes, **2**, exhibited a reduction potential at −0.88 V vs Ag/AgCl and −1.52 V vs Ag/AgCl, respectively. The DACH ligand substitution, contributed to shifting the potential by 0.02 V. This supports the stabilizing effect of the DACH ligands by coordinating Au(III) centers. An oxidation potential at 0.75 V vs Ag/AgCl for complexes **6** and **8** corresponds to ligand events, consistent with that of the starting material at 0.63 V. This is also an indication of the increased stability of the Au(III) center by the DACH ligand substitution. The complexes **6** and **8** had the same observed cyclic voltammogram regardless of the counterion present (Cl⁻

and BF$_4$⁻). All complexes displayed the increased stability of the Au(III) center by DACH ligand substitution. It will support the stability of these complexes in biological medium.

Computational Insight. To gain computational insight and molecular orbital configuration of these gold(III) complexes, we conducted DFT calculations. The energy optimization of complexes **3** and **6** was performed using the B3LYP (6-31G (d,p)) with SDD basis set. Crystal structures of both complexes were used as input coordinates. Frequency and MO calculations were performed using B3LYP/GenECP (6-31G(d,p)), Freq = HPMODES and scf = qc with the SDD basis set, where energy optimized files (Tables S3 and S4) were used as input. Figure 9A,B represents the important HOMO and LUMO plots for complex **3** and complex **6** respectively. The MO energies are shown in Tables S1 and S2. HOMO−LUMO gaps were found to be 4.388 and 1.825 eV for complexes **3** and **6** respectively. The HOMO−LUMO gap explains the lowest electronic excitation that is possible in a given molecule. We observed that **6** possessed a lower HOMO−LUMO gap compared to **3** and that may be attributed to the lack of efficient charge transfer in **3** owing to the absence of an acceptor moiety but the presence of two DACH donor ligands. Additionally, the distorted planarity associated with **3** contributes to the relatively larger band gap observed.

Furthermore, selected bond lengths of the computed structure and the crystal structure were compared for complexes **3** and **6**, as shown in Table 6. Both complexes
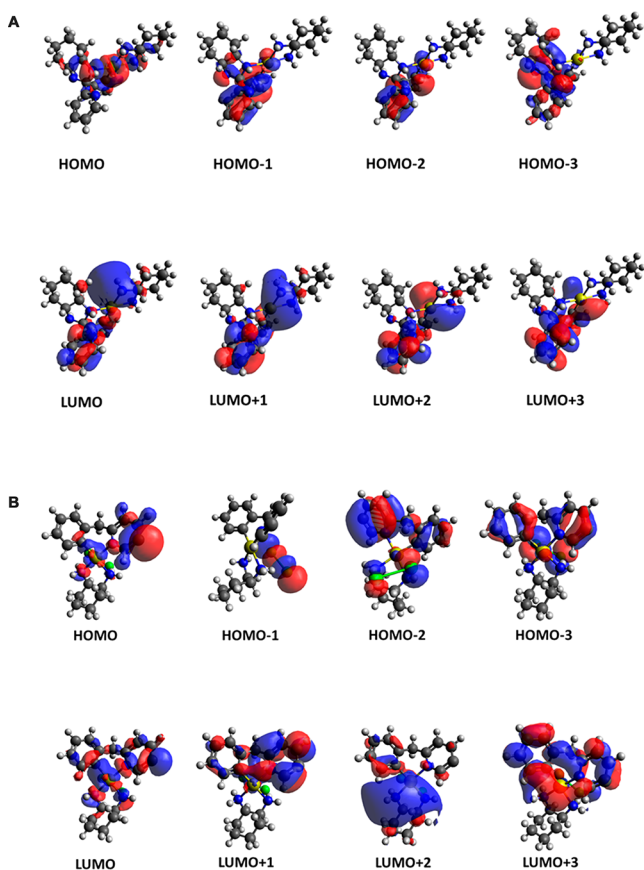
Figure 9. (A) Important molecular orbital (HOMO, LUMO) plot for complex **3**. (B) Important molecular orbital (HOMO, LUMO) plot for complex **6**.

Table 6. (a) Computed and Crystal Structure Bond Lengths of Complex 3 and (b) Computed and Crystal Structure Bond Lengths of Complex 6

(a)		
	calculated (Å)	crystal structure (Å)
Au1−C24	2.048	2.012
Au1−N2	2.490	2.026
Au1−N3	2.366	2.044
Au1−N1	2.274	2.126
N1−C1	1.479	1.486
N2−C2	1.494	1.497
N3−C13	1.531	1.523
N4−C13	1.471	1.469
C13−C14	1.546	1.538
(b)		
	calculated (Å)	crystal structure (Å)
Au1−N1	2.111	2.031
Au1−C1	2.064	2.031
Au1−N2	2.199	2.048
Au1−N3	2.221	2.109

exhibited similar bond lengths between the computed and crystal structures. This indicates that our crystal structure geometries match the computationally optimized molecular geometry and corroborates the computational method employed.

SUMMARY AND CONCLUSION

Six complexes have been synthesized and characterized, including a novel class of cyclometalated gold(III) compounds, **3**−**5**, of the type [Au(C^NH)(DACH)$_2$]$^+$ and the nitrogen substituted cyclometalated Au(III) compounds, **6**−**8**, of the type [Au(C^N)(DACH)]$^{2+}$. Electrochemical characterization of these complexes suggests that they are not reduced to metallic gold but display the conventional Au(III)/Au(I) redox couple. The X-ray crystal structure of the complexes reveals slightly distorted square-planar geometry, consistent with DFT computed structures. On the basis of our IC$_{50}$ values, complexes **3**−**5** displayed high potency toward the ovarian cancer cell lines, A2780 and OVCAR8, while complexes **6**−**8** were more potent in MCF7 and RPE MYC cells. Subsequently, insight into cell-cycle demonstrates significant arrest in the G1 phase for both classes of complexes, which is similar to auranofin. Cellular uptake of the complexes are well-differentiated from 200−1200 pmol/million cells, consistent with the moderate potency of the complexes observed in the OVCAR8 cell line. In support of the fact that DNA is an unlikely target of these complexes, interaction of **5** or **8** with plasmid DNA does not reveal nicking or smearing at complex concentrations lower than 500 μM. The complexes proved stable in DMEM over the course of 72 h, and also the reactivity with L-glutathione or ascorbate is moderate compared to other gold(III) complexes. We propose that the DACH ligand substitution to the gold(III) center increases stability of these complexes. These studies serve as a guide for enhanced Au(III) stabilization promoted by combined cyclometalation and DACH ligands that has the potential to impact gold-based anticancer drug design in the future.

EXPERIMENTAL SECTION

General Methods. All synthetic manipulations were performed under normal atmospheric conditions. HAuCl$_4$·3H$_2$O was purchased from Strem Chemicals and stored in a desiccator until use. Benzoylpyridine and benzylpyridine were purchased from Sigma-Aldrich, and (1R,2R)-(+)-1,2-diaminocyclohexane was purchased from TCI America and used without further purification. Deuterated solvents were purchased from Cambridge Isotope Laboratories (Andover, MA). ACS grade or higher solvents were used.

Physical Measurements. ^{1}H NMR, ^{13}C{^{1}H} NMR, and ^{19}F{^{1}H} NMR spectra were obtained on a 500 MHz Bruker spectrometer in the University of Kentucky NMR facility. Chemical shifts in ^{1}H NMR spectra were internally referenced to solvent signals (^{1}H NMR: DMSO at δ = 2.50 ppm and CD$_3$OD at δ = 3.31, ^{13}C NMR: DMSO at δ = 39.52 ppm and CD$_3$OD at δ = 49.00 ppm). A Shimadzu UV−vis spectrometer was used to acquire the UV−vis spectra. Elemental analyses (CHN) were carried out by the microanalysis laboratory at the University of Illinois at Urbana−Champaign. High-resolution mass spectra were obtained from BU Chemistry Department Chemical Instrumentation Center at Boston.

Synthetic Procedures. The cyclometalated gold(III) [Au(C^N)-(pcp)Cl$_2$] [pcp=2-(2-pyridyl carbonyl)phenyl] and [Au(C^N)(bpy)-Cl$_2$][81] [bpy=2-benzylpyridine] starting materials were prepared according to literature procedures.[27,29]

Synthesis of Complex 3 [Au(C^NH)(DACH)$_2$]$^+$ Cl$^-$. To a mixture of [AuCl^2(pcp-C′,N] [pcp = 2-(2-pyridyl carbonyl)phenyl] (154.7 mg, 0.34 mmol) and (1R,2R)-(+)-1,2-diaminocyclohexane (39.2 mg, 0.34 mmol) was added 5.0 mL of dichloromethane/methanol (1:1, v/v). The off-white suspension was stirred for 12 h at room temperature. The resulting clear solution was filtered through Celite, and the solvent was removed in vacuo. The residue was dissolved in a minimal amount of dichloromethane (2 mL), and hexane (10 mL) was added to precipitate the product at −20 °C. The resultant off-white precipitate was filtered under a vacuum and washed with diethyl ether

(3 × 10 mL) and dried in vacuo. ^{1}H NMR (400 MHz, methanol-d_4) δ 8.61 (dt, J = 4.9, 1.2 Hz, 1H), 8.15 (d, J = 7.9 Hz, 1H), 7.95 (**dtd**, J = 21.0, 7.7, 1.8 Hz, 1H), 7.50−7.25 (m, 5H), 7.21 (**ddd**, J = 13.4, 7.5, 1.6 Hz, 2H), 3.37 (s, 1H), 3.26 (td, J = 11.6, 4.2 Hz, 1H), 3.16−2.83 (m, 2H), 2.69−2.46 (m, 2H), 2.33 (dt, J = 15.8, 8.4 Hz, 2H), 2.30−2.18 (m, 1H), 2.21−2.14 (m, 1H), 1.96−1.84 (m, 1H), 1.80 (d, J = 9.8 Hz, 2H), 1.74−1.51 (m, 2H), 1.51 (d, J = 8.6 Hz, 1H), 1.43−1.38 (m, 1H), 1.38−1.25 (m, 4H). ^{13}C{^{1}H} NMR (101 MHz, methanol-d_4) δ 160.37, 152.77, 149.83, 149.44, 139.21, 138.84, 138.08, 130.70, 130.60, 130.34, 130.28, 130.02, 129.25, 127.61, 127.45, 125.03, 124.76, 121.71, 120.42, 100.96, 72.13, 69.35, 65.37, 63.41, 62.84, 60.79, 60.22, 34.44, 34.12, 33.40, 33.15, 32.79, 29.60, 29.35, 28.49, 25.70, 25.21, 24.81, 24.75, 24.72, 24.69, 24.64. Anal. % Calcd for $C_{24}H_{34}AuN_5Cl\cdot1.8$ CH_2Cl_2: C, 39.84%; H, 4.87%; N, 9.0%. Found: C, 39.84%; H, 4.91%; N, 9.12%.

Synthesis of Complex 4 [Au(C^NH)(DACH)$_2$]$^+$ ClO$_4^−$. The same procedure for synthesis of compound 3 was followed in the presence of 2 equimolar NaClO$_4$ salt to obtain a ClO$_4^−$ counterion. ^{1}H NMR (400 MHz, DMSO-d_6) δ 8.50 (d, J = 4.0 Hz, 1H), 8.32 (s, 2H), 8.04 (d, J = 8.0 Hz, 1H), 7.80 (d, J = 7.6 Hz, 1H), 7.33 (d, J = 7.4 Hz, 2H), 7.30−7.19 (m, 2H), 7.22−7.10 (m, 2H), 7.00 (d, J = 7.7 Hz, 2H), 3.38 (q, J = 7.0 Hz, 1H), 2.86 (d, J = 10.5 Hz, 4H), 2.42−2.33 (m, 2H), 2.16 (d, J = 9.4 Hz, 1H), 2.05 (q, J = 11.4 Hz, 5H), 1.93 (d, J = 10.2 Hz, 1H), 1.85 (d, J = 10.1 Hz, 4H), 1.73−1.62 (m, 1H), 1.63 (s, 9H), 1.45 (t, J = 12.1 Hz, 3H), 1.33 (d, J = 11.2 Hz, 1H), 1.27−1.13 (m, 15H), 1.09 (t, J = 7.0 Hz, 2H). ^{13}C{^{1}H} NMR (101 MHz, DMSO-d_6) δ 159.63, 156.62, 153.51, 152.46, 150.38, 150.09, 148.83, 148.75, 148.42, 138.26, 137.83, 137.68, 134.29, 133.60, 130.34, 130.16, 129.69, 129.30, 128.70, 127.98, 127.73, 127.32, 126.39, 126.33, 124.00, 123.81, 123.30, 119.33, 119.23, 99.47, 71.18, 71.06, 70.62, 67.86, 64.05, 63.19, 62.95, 51.37, 33.69, 32.72, 30.63, 28.86, 28.31, 27.19, 24.46, 23.74, 23.51, 23.40, 22.61 TOF-MS-ES$^+$: m/z (%) 588.2419 (100) [M − ClO$_4^−$]$^+$, calculated m/z for [M − ClO$_4^−$]$^+$ 588.2402.

Synthesis of Complex 5 [Au(C^NH)(DACH)$_2$]$^+$ BF$_4^−$. The same procedure of synthesis of compound 3 was followed in the presence of 2 equimolar NaBF$_4$ salt to obtain a BF$_4^−$ counterion. ^{1}H NMR (400 MHz, DMSO-d_6) δ 8.87 (d, J = 4.9 Hz, 1H), 8.68−8.54 (m, 3H), 8.48 (d, J = 10.0 Hz, 1H), 8.39 (d, J = 10.6 Hz, 1H), 8.17 (t, J = 6.9 Hz, 1H), 8.07 (d, J = 7.8 Hz, 1H), 8.02−7.86 (m, 5H), 7.80−7.35 (m, 11H), 7.36−7.09 (m, 5H), 7.12−6.91 (m, 3H), 6.78 (dd, J = 7.8, 1.5 Hz, 1H), 6.57−6.45 (m, 2H), 6.01 (dt, J = 22.8, 10.3 Hz, 3H), 4.39−4.22 (m, 3H), 4.04 (s, 1H), 3.19−3.10 (m, 2H), 3.11−3.00 (m, 2H), 2.91 (t, J = 10.8 Hz, 2H), 2.63 (s, 2H), 2.39 (q, J = 12.6 Hz, 1H), 2.19 (d, J = 12.0 Hz, 1H), 2.04 (s, 3H), 2.04−1.93 (m, 1H), 1.77 (d, J = 11.0 Hz, 1H), 1.67 (s, 8H), 1.55 (s, 1H), 1.52 (s, 4H), 1.45 (dd, J = 16.4, 12.4 Hz, 2H), 1.21 (d, J = 17.1 Hz, 11H), 1.12 (s, 1H), 0.82 (d, J = 12.4 Hz, 1H). ^{13}C{^{1}H} NMR (101 MHz, DMSO-d_6) δ 159.63, 156.62, 153.51, 152.46, 150.38, 150.09, 148.83, 148.75, 148.42, 138.26, 137.83, 137.68, 134.29, 133.60, 130.34, 130.16, 129.69, 129.30, 128.70, 127.98, 127.73, 127.32, 126.39, 126.33, 124.00, 123.81, 123.30, 119.33, 119.23, 99.47, 71.18, 71.06, 70.62, 67.86, 64.05, 63.19, 62.95, 51.37, 33.69, 32.72, 30.63, 28.86, 28.31, 27.19, 24.46, 23.74, 23.51, 23.40, 22.61 ^{19}F{^{1}H} NMR (377 MHz, DMSO-d_6) δ −148.29, −148.34 TOF-MS-ES$^+$: m/z (%) 588.2391 (100) [M − BF$_4^−$]$^+$, calculated m/z for [M − BF$_4^−$]$^+$ 588.2402.

Synthesis of Complex 6 [Au(C^N)(DACH)]$^{2+}$ 2Cl$^−$. Suspensions of cyclometalated gold 2 (74.2 mg, 0.17 mmol) and (1R,2R)-(+)-1,2-diaminocyclohexane (19.4 mg, 0.17 mmol) in 5.0 mL of dichloromethane/methanol (1:1, v/v) were stirred for 12 h at RT. The resultant clear solution was filtered through Celite, and solvent was evaporated from the filtrate. The resultant crude product was recrystallized with methanol to obtain the desired product (80 mg, 0.15 mmol, 85.62% yield). ^{1}H NMR (400 MHz, DMSO-d_6) δ 9.47 (s, 1H), 8.30 (td, J = 7.7, 1.5 Hz, 1H), 8.06 (dd, J = 7.9, 1.5 Hz, 1H), 7.75−7.67 (m, 1H), 7.61 (s, 2H), 7.35 (dd, J = 7.5, 1.6 Hz, 1H), 7.25 (t, J = 7.3 Hz, 1H), 7.12 (td, J = 7.6, 1.6 Hz, 1H), 6.66 (s, 1H), 5.66 (s, 1H), 5.10 (s, 1H), 4.40 (s, 1H), 3.29−3.21 (m, 1H), 3.04−2.93 (m, 1H), 2.07 (s, 3H), 1.63 (d, J = 10.0 Hz, 3H), 1.32 (s, 1H), 1.21 (s, 0H), 1.20−1.08 (m, 2H). ^{13}C{^{1}H} NMR (101 MHz, DMSO-d_6) δ

156.61, 143.24, 133.77, 128.31, 128.02, 126.68, 124.45, 45.91, 39.94, 39.73, 39.52, 39.31, 39.10, 38.89, 38.69, 33.49, 31.81, 23.94, 23.62. Anal. % Calcd for $C_{18}H_{24}AuN_3Cl_2$ 0.75CH_2Cl_2: C, 36.68%; H, 4.19%; N, 6.84%. Found: C, 36.53%; H, 4.46%; N, 6.93%.

Synthesis of Complex 7 [Au(C^N)(DACH)]$^{2+}$ 2ClO$_4^−$. The same procedure for synthesis of compound 6 was followed in the presence of 2 equimolar NaClO$_4$ salt to obtain a ClO$_4^−$ counterion. ^{1}H NMR (400 MHz, DMSO-d_6) δ 9.36 (s, 1H), 8.29 (td, J = 7.7, 1.5 Hz, 1H), 8.05 (dd, J = 7.9, 1.5 Hz, 1H), 7.71 (**ddd**, J = 7.5, 5.8, 1.5 Hz, 1H), 7.59 (s, 1H), 7.34 (dd, J = 7.5, 1.6 Hz, 1H), 7.24 (td, J = 7.3, 1.1 Hz, 1H), 7.12 (td, J = 7.6, 1.6 Hz, 1H), 6.52 (s, 1H), 5.61 (s, 1H), 4.91 (s, 1H), 4.47 (s, 1H), 3.19 (d, J = 12.5 Hz, 1H), 2.90 (s, 1H), 2.08−2.03 (m, 2H), 1.62 (s, 2H), 1.50 (s, 1H), 1.32 (s, 1H), 1.18−1.04 (m, 3H). ^{13}C{^{1}H} NMR (101 MHz, DMSO-d_6) δ 191.57, 157.35, 148.73, 129.23, 127.57, 125.36, 110.24, 110.22, 46.71, 40.77, 40.56, 40.36, 40.15, 39.94, 39.73, 39.52, 32.83, 24.81, 24.45, 0.06, −0.54. TOF-MS-ES$^+$: m/z (%) 478.1591 (100) [M + H]$^+$, calculated m/z for [M + H]$^+$ 478.1558.

Synthesis of Complex 8 [Au(C^N)(DACH)]$^{2+}$ 2BF$_4^−$. The same procedure for synthesis of compound 6 was followed in the presence of 2 equimolar NaBF$_4$ salt to obtain a BF$_4^−$ counterion. ^{1}H NMR (400 MHz, DMSO-d_6) δ 9.45 (s, 1H), 8.30 (td, J = 7.7, 1.5 Hz, 1H), 8.06 (dd, J = 8.0, 1.5 Hz, 1H), 7.71 (t, J = 6.8 Hz, 1H), 7.59 (s, 2H), 7.35 (dd, J = 7.5, 1.6 Hz, 1H), 7.25 (t, J = 7.3 Hz, 1H), 7.12 (td, J = 7.6, 1.6 Hz, 1H), 6.64 (s, 1H), 5.60 (s, 1H), 5.04 (s, 1H), 4.40 (s, 1H), 2.96 (t, J = 9.9 Hz, 1H), 2.07 (s, 2H), 1.63 (d, J = 10.3 Hz, 2H), 1.32−1.26 (m, 2H), 1.22−1.10 (m, 2H). ^{13}C{^{1}H} NMR (101 MHz, DMSO-d_6) δ 156.20, 151.43, 142.82, 133.35, 131.77, 127.89, 127.60, 126.26, 124.03, 62.73, 56.95, 45.49, 39.52, 39.31, 39.10, 38.89, 38.69, 38.48, 38.27, 33.07, 31.39, 23.52, 23.20. ^{19}F{^{1}H} NMR (377 MHz, DMSO-d_6) δ −148.13, −148.18, −148.23, −148.26, −148.28, −148.35, −148.40. TOF-MS-ES$^+$: m/z (%) 479.1642 (100) [M + H]$^+$, calculated m/z for [M + H]$^+$ 479.1636.

X-ray Crystallography. Low temperature (90K) X-ray diffraction data for 3, 5, and 8 were collected on a Bruker D8 Venture dual-source diffractometer, and the summary of the crystallographic information is given in Table 1. Crystals of 3, 5, and 8 were grown at room temperature by vapor diffusion of diethyl ether into DMF or MeOH solutions of each complex. All crystals were mounted using polyisobutene oil on the tip of a fine glass fiber, which was fastened in a copper mounting pin with an electrical solder. It was placed directly into the cold gas stream of a liquid-nitrogen based cryostat.[82,83] Raw data were integrated, scaled, merged, and corrected for Lorentz-polarization effects using the APEX3 package.[84−86] Space group determination and structure solution and refinement were carried out with SHELXT and SHELXL,[87,88] respectively. All non-hydrogen atoms were refined with anisotropic displacement parameters. Hydrogen atoms were placed at calculated positions and refined using a riding model with their isotropic displacement parameters (U_{iso}) set to either 1.2U_{iso} or 1.5U_{iso} of the atom to which they were attached. Ellipsoid plots were drawn using SHELXTL-XP.[89] The structures, deposited in the Cambridge Structural Database, were checked for missed symmetry, twinning, and overall quality with PLATON,[90] an R-tensor,[91] and finally validated using CheckCIF.[90]

Solution Studies. A 1.5 mM stock solution of complex 3 (1 mg, 1.5 μmol) or 1.8 mM of complex 6 (1 mg, 1.8 μmol) in DMSO (1 mL) was prepared. The stock solution of complex 3 (334 μL) was further diluted with DMSO (166 μL) to achieve 1 mM gold solution (500 μL). Similarly, the stock solution of complex 6 (275 μL) was further diluted with DMSO (225 μL) to achieve 1 mM gold solution (500 μL). Subsequently, 250 μL of a 1 mM solution of complex 3 or complex 6 and 4.75 mL of DMEM were combined in a cuvette, and UV−vis spectra were recorded hourly for the first 72 h uninterruptedly. Note, the final concentration of both complexes 3 or 6 were 50 μM in DMEM. In all time points, DMEM with 5% DMSO was used as background to correct for absorption from DMEM and DMSO.[77]

Reaction with Glutathione. *NMR Experiment.* A 10.0 mM stock solution of complex 5 or complex 8 in DMSO-d_6 was prepared. In a separate vial a 100 mM stock solution of L-glutathione in DMSO-d_6

was also prepared. Subsequently, equal volumes of both L-glutathione (0.5 mL) and complex **5** or **8** (0.5 mL) from the stock solutions were combined in an NMR tube, and ^{1}H NMR spectra were recorded at 0 h, 1 h, 2 h, 4 h, and 12 h. Note the final concentration of both complex **5** or **8** and L-glutathione measured were 5 mM and 50 mM, respectively, achieving a ratio of 1:10.

UV–vis Experiment. A 7.4 mM stock solution of complex **5** (1 mg, 1.5 μmol) or 7.7 mM of complex **8** (1 mg, 1.5 μmol) in DMSO (200 μL) was prepared. The stock solutions (0.13 mL) were diluted with DMEM (9.8 mL) to achieve 100 μM gold solutions (10 mL). In a separate vial, a 2 mM stock solution of L-glutathione (9.2 mg, 30 μmol) in DMEM (15 mL) was also prepared. Subsequently, equal volumes of both **5** or **8** solutions (2 mL) and L-glutathione (2 mL) from the prepared stock solutions were combined in a cuvette, and UV–vis spectra were recorded hourly for the first 12 h uninterruptedly and then 24 h in a controlled manner. Note the final concentrations of both complex **5** or **8** and L-glutathione measured were 50 μM and 1 mM respectively, achieving a ratio of 1:20. In all time points, DMEM with 0.0013% DMSO was used as a background to correct for absorption from DMEM and DMSO.

Reaction with Ascorbate. UV–vis Experiment. Similarly, a 7.4 mM stock solution of complex **5** (1 mg, 1.5 μmol) or 7.7 mM of complex **8** (1 mg, 1.5 μmol) in DMSO (200 μL) was prepared. The stock solutions (0.13 mL) were diluted with DMEM (9.8 mL) to achieve 100 μM gold solutions (10 mL). In a separate vial, a 2 mM stock solution of sodium ascorbate (5.94 mg, 30 μmol) in DMEM (15 mL) was also prepared. Subsequently, equal volumes of both **5** or **8** solutions (2 mL) and sodium ascorbate (2 mL) from the prepared stock solutions were combined in a cuvette, and UV–vis spectra were recorded hourly for the first 12 h uninterruptedly and then 24 h in a controlled manner. Note the final concentrations of both complex **5** or **8** and ascorbate measured were 50 μM and 1 mM respectively, achieving a ratio of 1:20. In all time points, DMEM with 0.0013% DMSO was used as a background to correct for absorption from DMEM and DMSO.

DNA Interaction Studies. DNA interaction ability of complexes **3** and **6** were determined by using agarose gel electrophoresis. DNA was extracted from pUC19 plasmid. Solutions containing 10 ng/mL DNA and 1000, 500, 250, 125, 62.5, and 0 μM of compound **3** with a total volume of 15 μL in TE buffer were incubated for 20 h at 37 °C. After the incubation, 15 μL of purple loading dye was added, and reaction mixtures were immediately loaded to a 1% agarose gel containing 10 μL of 1 mg/mL ethidium bromide. The first lane of the gel was loaded with a mixture of 15 μL ladder and 15 μL purple loading dye. The gel was run by applying 76 V for 2 h by using 1xTAE buffer as a running buffer.[77] The DNA band was analyzed under UV light using a BioRad Gel Imager. The same method was repeated for compound **6**.

Cell Culture. A2780 and OVCAR8 ovarian cancer cell lines were purchased from ATCC and cultured in RPMI 1640 medium with 10% FBS, 2 mM L-glutamine, 100 units/mL penicillin, and 100 μg/mL streptomycin (Invitrogen). All cells were maintained at 37 °C in a humid atmosphere containing 5% CO_2. The human fetal fibroblast (MRC5) cells, MCF7 and RPE MYC cell lines were cultured in DMEM with 10% FBS, 2 mM L-glutamine, 100 units/mL penicillin, and 100 μg/mL streptomycin (Invitrogen). Cells were maintained at 37 °C in a humid atmosphere containing 5% CO_2.

Cell Viability Studies Using Crystal Violet Assay. Cells (2 × 10^3) were seeded in each well of a 96-well plate. After the cells were incubated overnight, various concentrations of test compound (0.13–100 μM) were added and incubated for 48 h (total volume 2 mL). After 48 h, one designated well was treated with 2 mM of H_2O_2 and again incubated for 3 h at 37 °C. The cells were then stained with 50 μL of crystal violet solution for 1 h, rinsed, and air-dried. A total of 200 μL of methanol was added to each well, and the absorbance of the solution wells was read at 570 nm. Absorbance values were normalized to the control well as 100% and plotted as a concentration of test compound versus % cell viability.

Cell Cycle Analysis - OVCAR 8 Cell Line. Cells (5 × 10^5) were seeded in each well of a six-well (15 wells) plate. After the cells were

incubated overnight, 5 μM of complex **5** for three wells and complex **8** for three wells were added, and three wells were kept without adding compounds and incubated at 37 °C. After 24 h incubation, one control and each well per sample were harvested via trypsinization and centrifuged to form a pellet. The pellet was washed with PBS and transferred to 1.5 mL centrifuge tubes and centrifuged to form a pellet. Then the PBS was decanted, and the pellet was resuspended in 1.0 mL of 70% ethanol in PBS and stored in 4 °C. The same procedure was followed to collect the 48 and 72 h time points.

After the collection of all time points, collected pellets were washed twice with 1.0 mL of PBS. A total of 50 μL of 100 μg/mL RNase solution and 200 μL of 50 μg/mL propidium iodide solution were added to each sample and resuspended, and cells were filtered via a strainer. All the samples were analyzed with flow cytometry.

Whole Cell Uptake. OVCAR8 cells (5 × 10^5) were seeded in each well of a six-well plate. After the cells were incubated overnight, 10 μM of cisplatin for two wells, auranofin for two wells, complex **5** for two wells, and complex **8** for two wells and incubated at 37 °C for 15 h. Cells were collected via trypsinization and transferred to a 15 mL centrifuge tube and centrifuged for 5 min, and the pellets were transferred to 1.5 mL centrifuge tubes. Pellets were washed twice with PBS and then resuspended in 0.5 mL con. HCl and agitated for 30 s. Solutions were transferred to 15 mL tubes containing 4.5 mL DI water to make the HCl concentration 10%. Samples were analyzed with ICP-OES to get the concentration of gold in each sample.

Apoptosis Analysis - OVCAR8 Cell Line. Cells (5 × 10^5) were seeded in each well of a six-well (10 wells) plate. After the cells were incubated overnight, 10 μM of cisplatin for two wells, auranofin for two wells, complex **5** for two wells, and complex **8** for two wells were added, and two wells were kept without adding compounds and incubated for 72 h (total volume 2 mL). After 72 h, one designated well was treated with 2 μM of H_2O_2 and again incubated for 3 h at 37 °C. Then the media was transferred to labeled 15.0 mL centrifuge tubes and were washed with 1.0 mL PBS and transferred to labeled centrifuge tubes. Cells were harvested via trypsinization and transferred to labeled centrifuge tubes. Tubes were centrifuged for 5 min to form a pellet. The supernatant was decanted, cell pellets were resuspended in 5.0 mL of media, and cells were counted and made a new solution of 1 × 10^5 cells/ml solution were made for each sample separately. New cell solution was transferred to 1.5 mL centrifuge tube and centrifuged to form a pellet. Pellets were resuspended in 500 μL annexin binding buffer. Five microliters of propidium iodide and 5 μL of annexin V-FITC were added to each tube and incubated in the dark for 5 min and analyzed with flow cytometry.

Electrochemistry. 1.0 mM solutions of ligand alone, gold(III) starting materials alone, and gold(III)–DACH compounds were prepared by dissolving the compounds in DMSO. 0.1 M NaClO$_4$·H_2O was added as an electrolyte. Electrochemical measurements were performed at RT by using CH instruments 650E potentiostat, which contains custom 3 electrodes cell comprised of a 3 mm diameter glassy-carbon working electrode, platinum-wire counter electrode, and freshly anodized Ag/AgCl wire reference electrode. Ferrocene was used as an internal reference.

■ **ASSOCIATED CONTENT**

Ⓢ **Supporting Information**

The Supporting Information is available free of charge on the ACS Publications website at DOI: 10.1021/acs.inorg-chem.9b01031.

> A list of characterization data including NMR spectroscopy, mass spectrometry and HPLC trace of compounds as well as dose response curves, UV–vis spectra, cyclic voltammograms (PDF)

Accession Codes

CCDC 1906370−1906372 contain the supplementary crystallographic data for this paper. These data can be obtained free of charge via www.ccdc.cam.ac.uk/data_request/cif, or by

emailing data_request@ccdc.cam.ac.uk, or by contacting The Cambridge Crystallographic Data Centre, 12 Union Road, Cambridge CB2 1EZ, UK; fax: +44 1223 336033.

■ AUTHOR INFORMATION

Corresponding Author
*E-mail: awuah@uky.edu.

ORCID ●
Samuel G. Awuah: 0000-0003-4947-7283

■ REFERENCES

(1) Mjos, K. D.; Orvig, C. Metallodrugs in Medicinal Inorganic Chemistry. *Chem. Rev.* **2014**, *114* (8), 4540–4563.
(2) Dasari, S.; Bernard Tchounwou, P. Cisplatin in cancer therapy: Molecular mechanisms of action. *Eur. J. Pharmacol.* **2014**, *740*, 364–378.
(3) Lippert, B. *Cisplatin: Chemistry and Biochemistry of a Leading Anticancer Drug*; Wiley-VCH: Zürich, 1999.
(4) Wang, D.; Lippard, S. J. Cellular processing of platinum anticancer drugs. *Nat. Rev. Drug Discovery* **2005**, *4*, 307.
(5) Muggia, F. M.; Bonetti, A.; Hoeschele, J. D.; Rozencweig, M.; Howell, S. B. Platinum Antitumor Complexes: 50 Years Since Barnett Rosenberg's Discovery. *J. Clin. Oncol.* **2015**, *33*, 4219–4226.
(6) McWhinney, S. R.; Goldberg, R. M.; McLeod, H. L. Platinum neurotoxicity pharmacogenetics. *Mol. Cancer Ther.* **2009**, *8* (1), 10–16.
(7) Ott, I.; Gust, R. Non Platinum Metal Complexes as Anti-cancer Drugs. *Arch. Pharm.* **2007**, *340* (3), 117–126.
(8) Romero-Canelón, I.; Sadler, P. J. Next-Generation Metal Anticancer Complexes: Multitargeting via Redox Modulation. *Inorg. Chem.* **2013**, *52* (21), 12276–12291.
(9) Huang, K.-B.; Wang, F.-Y.; Tang, X.-M.; Feng, H.-W.; Chen, Z.-F.; Liu, Y.-C.; Liu, Y.-N.; Liang, H. Organometallic Gold(III) Complexes Similar to Tetrahydroisoquinoline Induce ER-Stress-Mediated Apoptosis and Pro-Death Autophagy in A549 Cancer Cells. *J. Med. Chem.* **2018**, *61* (8), 3478–3490.

(10) Casado, R.; Contel, M.; Laguna, M.; Romero, P.; Sanz, S. Organometallic Gold(III) Compounds as Catalysts for the Addition of Water and Methanol to Terminal Alkynes. *J. Am. Chem. Soc.* **2003**, *125* (39), 11925–11935.
(11) Messina, M. S.; Stauber, J. M.; Waddington, M. A.; Rheingold, A. L.; Maynard, H. D.; Spokoyny, A. M. Organometallic Gold(III) Reagents for Cysteine Arylation. *J. Am. Chem. Soc.* **2018**, *140* (23), 7065–7069.
(12) Maia, P. I. d. S.; Carneiro, Z. A.; Lopes, C. D.; Oliveira, C. G.; Silva, J. S.; de Albuquerque, S.; Hagenbach, A.; Gust, R.; Deflon, V. M.; Abram, U. Organometallic gold(iii) complexes with hybrid SNS-donating thiosemicarbazone ligands: cytotoxicity and anti-Trypanosoma cruzi activity. *Dalton Trans.* **2017**, *46* (8), 2559–2571.
(13) Lopes, C. D.; Gaspari, A. P. S.; Oliveira, R. J.; Abram, U.; Almeida, J. P. A.; Maia, P. I. d. S.; da Silva, J.; de Albuquerque, S.; Carneiro, Z. A. Organometallic gold(III) [Au(Hdamp)(L1⁴)]Cl (L1 = SNS-donating thiosemicarbazone) complex protects mice against acute T. cruzi infection. *bioRxiv* **2018**, 312702.
(14) Wu, C.-Y.; Horibe, T.; Jacobsen, C. B.; Toste, F. D. Stable gold(III) catalysts by oxidative addition of a carbon–carbon bond. *Nature* **2015**, *517*, 449.
(15) Sadler, P. J.; Sue, R. E. The Chemistry of Gold Drugs. *Metal-Based Drugs* **1994**, *1* (2–3), 107–144.
(16) Hashmi, A. S. K.; Blanco, M. C.; Fischer, D.; Bats, J. W. Gold Catalysis: Evidence for the In-situ Reduction of Gold(III) During the Cyclization of Allenyl Carbinols. *Eur. J. Org. Chem.* **2006**, *2006* (6), 1387–1389.
(17) Wolf, W. J.; Winston, M. S.; Toste, F. D. Exceptionally fast carbon–carbon bond reductive elimination from gold(III). *Nat. Chem.* **2014**, *6*, 159.
(18) Zou, T.; Lum, C. T.; Lok, C.-N.; Zhang, J.-J.; Che, C.-M. Chemical biology of anticancer gold(iii) and gold(i) complexes. *Chem. Soc. Rev.* **2015**, *44* (24), 8786–8801.
(19) Kumar, R.; Nevado, C. Cyclometalated Gold(III) Complexes: Synthesis, Reactivity, and Physicochemical Properties. *Angew. Chem., Int. Ed.* **2017**, *56* (8), 1994–2015.
(20) Tang, M.-C.; Tsang, D. P.-K.; Wong, Y.-C.; Chan, M.-Y.; Wong, K. M.-C.; Yam, V. W.-W. Bipolar Gold(III) Complexes for Solution-Processable Organic Light-Emitting Devices with a Small Efficiency Roll-Off. *J. Am. Chem. Soc.* **2014**, *136* (51), 17861–17868.
(21) To, W.-P.; Tong, G. S. M.; Cheung, C.-W.; Yang, C.; Zhou, D.; Che, C.-M. Luminescent Cyclometalated Gold(III) Alkyl Complexes: Photophysical and Photochemical Properties. *Inorg. Chem.* **2017**, *56* (9), 5046–5059.
(22) Blons, C.; Mallet-Ladeira, S.; Amgoune, A.; Bourissou, D. (P,C) Cyclometalated Gold(III) Complexes: Highly Active Catalysts for the Hydroarylation of Alkynes. *Angew. Chem., Int. Ed.* **2018**, *57* (36), 11732–11736.
(23) Szentkuti, A.; Garg, J. A.; Blacque, O.; Venkatesan, K. Monocyclometalated Gold(III) Complexes Bearing π-Accepting Cyanide Ligands: Syntheses, Structural, Photophysical, and Electrochemical Investigations. *Inorg. Chem.* **2015**, *54* (22), 10748–10760.
(24) Rekhroukh, F.; Blons, C.; Estévez, L.; Mallet-Ladeira, S.; Miqueu, K.; Amgoune, A.; Bourissou, D. Gold(iii)–arene complexes by insertion of olefins into gold–aryl bonds. *Chem. Sci.* **2017**, *8* (6), 4539–4545.
(25) Serra, J.; Font, P.; Sosa Carrizo, E. D.; Mallet-Ladeira, S.; Massou, S.; Parella, T.; Miqueu, K.; Amgoune, A.; Ribas, X.; Bourissou, D. Cyclometalated gold(iii) complexes: noticeable differences between (N,C) and (P,C) ligands in migratory insertion. *Chem. Sci.* **2018**, *9* (16), 3932–3940.
(26) Rekhroukh, F.; Brousses, R.; Amgoune, A.; Bourissou, D. Cationic Gold(III) Alkyl Complexes: Generation, Trapping, and Insertion of Norbornene. *Angew. Chem., Int. Ed.* **2015**, *54* (4), 1266–1269.
(27) Kung, K. K.-Y.; Lo, V. K.-Y.; Ko, H.-M.; Li, G.-L.; et al. Cyclometallated Gold(III) Complexes as Effective Catalysts for Synthesis of Propargylic Amines, Chiral Allenes and Isoxazoles. *Adv. Syn. & Catal.* **2013**, *355* (10), 2055–2070.

(28) Au, V. K.-M.; Wong, K. M.-C.; Zhu, N.; Yam, V. W.-W. Luminescent Cyclometalated Dialkynylgold(III) Complexes of 2-Phenylpyridine-Type Derivatives with Readily Tunable Emission Properties. *Chem. - Eur. J.* **2011**, *17* (1), 130−142.

(29) Shaw, A. P.; Tilset, M.; Heyn, R. H.; Jakobsen, S. Microwave methods for the synthesis of gold(III) complexes. *J. Coord. Chem.* **2011**, *64* (1), 38−47.

(30) Glisic, B. D.; Rychlewska, U.; Djuran, M. I. Reactions and structural characterization of gold(iii) complexes with amino acids, peptides and proteins. *Dalton Trans.* **2012**, *41* (23), 6887−6901.

(31) Fuchita, Y.; Ieda, H.; Tsunemune, Y.; Kinoshita-Nagaoka, J.; Kawano, H. Synthesis, structure and reactivity of a new six-membered cycloaurated complex of 2-benzoylpyridine [AuCl₂(pcp-C 1,N)] [pcp = 2-(2-pyridylcarbonyl)phenyl]. Comparison with the cycloaurated complex derived from 2-benzylpyridine. *J. Chem. Soc., Dalton Trans.* **1998**, No. 5, 791−796.

(32) Cinellu, M. A.; Minghetti, G.; Pinna, M. V.; Stoccoro, S.; Zucca, A.; Manassero, M. Gold(III) derivatives with anionic oxygen ligands: mononuclear hydroxo, alkoxo and acetato complexes. Crystal structure of [Au(bpy)(OMe)2][PF6]. *J. Chem. Soc., Dalton Trans.* **2000**, No. 8, 1261−1265.

(33) Parish, R. V.; Howe, B. P.; Wright, J. P.; Mack, J.; Pritchard, R. G.; Buckley, R. G.; Elsome, A. M.; Fricker, S. P. Chemical and Biological Studies of Dichloro(2-((dimethylamino)methyl)phenyl)-gold(III). *Inorg. Chem.* **1996**, *35* (6), 1659−1666.

(34) Buckley, R. G.; Elsome, A. M.; Fricker, S. P.; Henderson, G. R.; Theobald, B. R. C.; Parish, R. V.; Howe, B. P.; Kelland, L. R. Antitumor Properties of Some 2-[(Dimethylamino)methyl]-phenylgold(III) Complexes. *J. Med. Chem.* **1996**, *39* (26), 5208−5214.

(35) Zhang, J.-J.; Sun, R. W.-Y.; Che, C.-M. A dual cytotoxic and anti-angiogenic water-soluble gold(iii) complex induces endoplasmic reticulum damage in HeLa cells. *Chem. Commun.* **2012**, *48* (28), 3388−3390.

(36) Bertrand, B.; Fernandez-Cestau, J.; Angulo, J.; Cominetti, M. M. D.; Waller, Z. A. E.; Searcey, M.; O'Connell, M. A.; Bochmann, M. Cytotoxicity of Pyrazine-Based Cyclometalated (C^Npz^C)Au(III) Carbene Complexes: Impact of the Nature of the Ancillary Ligand on the Biological Properties. *Inorg. Chem.* **2017**, *56* (10), 5728−5740.

(37) Williams, M.; Green, A. I.; Fernandez-Cestau, J.; Hughes, D. L.; O'Connell, M. A.; Searcey, M.; Bertrand, B.; Bochmann, M. (C^Npz^C)AuIII complexes of acyclic carbene ligands: synthesis and anticancer properties. *Dalton Trans.* **2017**, *46* (39), 13397−13408.

(38) Johnson, M. W.; DiPasquale, A. G.; Bergman, R. G.; Toste, F. D. Synthesis of Stable Gold(III) Pincer Complexes with Anionic Heteroatom Donors. *Organometallics* **2014**, *33* (16), 4169−4172.

(39) Bertrand, B.; Williams, M. R. M.; Bochmann, M. Gold(III) Complexes for Antitumor Applications: An Overview. *Chem. - Eur. J.* **2018**, *24* (46), 11840−11851.

(40) Holmsen, M. S. M.; Nova, A.; Hylland, K.; Wragg, D. S.; Øien-Ødegaard, S.; Heyn, R. H.; Tilset, M. Synthesis of a (N,C,C) Au(iii) pincer complex via Csp3−H bond activation: increasing catalyst robustness by rational catalyst design. *Chem. Commun.* **2018**, *54* (79), 11104−11107.

(41) Williams, M. R. M.; Bertrand, B.; Fernandez-Cestau, J.; Waller, Z. A. E.; O'Connell, M. A.; Searcey, M.; Bochmann, M. Acridine-decorated cyclometallated gold(iii) complexes: synthesis and anti-tumour investigations. *Dalton Trans.* **2018**, *47* (38), 13523−13534.

(42) Wong, K.-H.; Cheung, K.-K.; Chan, M. C.-W.; Che, C.-M. Application of 2,6-Diphenylpyridine as a Tridentate [C^N^C] Dianionic Ligand in Organogold(III) Chemistry. Structural and Spectroscopic Properties of Mono- and Binuclear Transmetalated Gold(III) Complexes. *Organometallics* **1998**, *17* (16), 3505−3511.

(43) Fernandez-Cestau, J.; Bertrand, B.; Blaya, M.; Jones, G. A.; Penfold, T. J.; Bochmann, M. Synthesis and luminescence modulation of pyrazine-based gold(iii) pincer complexes. *Chem. Commun.* **2015**, *51* (93), 16629−16632.

(44) Messori, L.; Abbate, F.; Marcon, G.; Orioli, P.; Fontani, M.; Mini, E.; Mazzei, T.; Carotti, S.; O'Connell, T.; Zanello, P. Gold(III) Complexes as Potential Antitumor Agents: Solution Chemistry and Cytotoxic Properties of Some Selected Gold(III) Compounds. *J. Med. Chem.* **2000**, *43* (19), 3541−3548.

(45) Gabbiani, C.; Casini, A.; Messori, L. Gold(III) compounds as anticancer drugs. *Gold Bull.* **2007**, *40* (1), 73−81.

(46) Marcon, G.; Carotti, S.; Coronnello, M.; Messori, L.; Mini, E.; Orioli, P.; Mazzei, T.; Cinellu, M. A.; Minghetti, G. Gold(III) Complexes with Bipyridyl Ligands: Solution Chemistry, Cytotoxicity, and DNA Binding Properties. *J. Med. Chem.* **2002**, *45* (8), 1672−1677.

(47) Carboni, S.; Zucca, A.; Stoccoro, S.; Maiore, L.; Arca, M.; Ortu, F.; Artner, C.; Keppler, B. K.; Meier-Menches, S. M.; Casini, A.; Cinellu, M. A. New Variations on the Theme of Gold(III) C∧N∧N Cyclometalated Complexes as Anticancer Agents: Synthesis and Biological Characterization. *Inorg. Chem.* **2018**, *57* (23), 14852−14865.

(48) Guenther, J.; Mallet-Ladeira, S.; Estevez, L.; Miqueu, K.; Amgoune, A.; Bourissou, D. Activation of Aryl Halides at Gold(I): Practical Synthesis of (P,C) Cyclometalated Gold(III) Complexes. *J. Am. Chem. Soc.* **2014**, *136* (5), 1778−1781.

(49) Wilson, J. J.; Lippard, S. J. Synthetic Methods for the Preparation of Platinum Anticancer Complexes. *Chem. Rev.* **2014**, *114* (8), 4470−4495.

(50) Al-Jaroudi, S. S.; Monim-ul-Mehboob, M.; Altaf, M.; Fettouhi, M.; Wazeer, M. I. M.; Altuwaijri, S.; Isab, A. A. Synthesis, spectroscopic characterization, X-ray structure and electrochemistry of new bis(1,2-diaminocyclohexane)gold(iii) chloride compounds and their anticancer activities against PC3 and SGC7901 cancer cell lines. *New J. Chem.* **2014**, *38* (7), 3199−3211.

(51) Trost, B. M.; Fandrick, D. R.; Dinh, D. C. Dynamic Kinetic Asymmetric Allylic Alkylations of Allenes. *J. Am. Chem. Soc.* **2005**, *127* (41), 14186−14187.

(52) Trost, B. M.; Xie, J.; Sieber, J. D. The Palladium Catalyzed Asymmetric Addition of Oxindoles and Allenes: An Atom-Economical Versatile Method for the Construction of Chiral Indole Alkaloids. *J. Am. Chem. Soc.* **2011**, *133* (50), 20611−20622.

(53) Casini, A.; Hartinger, C.; Gabbiani, C.; Mini, E.; Dyson, P. J.; Keppler, B. K.; Messori, L. Gold(III) compounds as anticancer agents: Relevance of gold−protein interactions for their mechanism of action. *J. Inorg. Biochem.* **2008**, *102* (3), 564−575.

(54) Al-Jaroudi, S. S.; Fettouhi, M.; Wazeer, M. I. M.; Isab, A. A.; Altuwaijri, S. Synthesis, characterization and cytotoxicity of new gold(III) complexes with 1,2-diaminocyclohexane: Influence of stereochemistry on antitumor activity. *Polyhedron* **2013**, *50* (1), 434−442.

(55) Cinellu, M. A.; Zucca, A.; Stoccoro, S.; Minghetti, G.; Manassero, M.; Sansoni, M. Synthesis and characterization of gold(III) adducts and cyclometallated derivatives with 2-substituted pyridines. Crystal structure of [Au{NC5H4(CMe2C6H4)-2}Cl2]. *J. Chem. Soc., Dalton Trans.* **1995**, No. 17, 2865−2872.

(56) Omer, K. H.; Seliman, A. A. A.; Al-Mohsin, H. A.; Kawde, A.-N.; Altaf, M.; Wazeer, M. I. M.; Ahmad, S.; Musa, M. M.; Isab, A. A. Study of the Interaction of Some Potential Anticancer Gold(III) Complexes with Biologically Important Thiols Using NMR, UV−Vis, and Electrochemistry. *Int. J. Chem. Kinet.* **2017**, *49* (6), 387−397.

(57) Sulaiman, A. A.; Omer, K. H.; Kawde, A.-N.; Wazeer, M. I. M.; Altaf, M.; Musa, M. M.; Ahmad, S.; Isab, A. A. Spectroscopic and Electrochemical Studies of the Interaction of Some Gold(III) Complexes with Biologically Relevant Thiones. *Int. J. Chem. Kin.* **2018**, *50* (3), 178−187.

(58) Djeković, A.; Petrović, B.; Bugarčić, Ž. D.; Puchta, R.; van Eldik, R. Kinetics and mechanism of the reactions of Au(iii) complexes with some biologically relevant molecules. *Dalton Trans.* **2012**, *41* (13), 3633−3641.

(59) Bertrand, B.; Casini, A. A golden future in medicinal inorganic chemistry: the promise of anticancer gold organometallic compounds. *Dalton Trans.* **2014**, *43* (11), 4209−4219.

(60) Roder, C.; Thomson, M. J. Most studies proved that gold (III) complexes interact with protein, not with DNA to cause cell death. *Drugs R&D* **2015**, *15* (1), 13−20.

(61) Vergara, E.; Casini, A.; Sorrentino, F.; Zava, O.; Cerrada, E.; Rigobello, M. P.; Bindoli, A.; Laguna, M.; Dyson, P. J. Anticancer Therapeutics That Target Selenoenzymes: Synthesis, Characterization, in vitro Cytotoxicity, and Thioredoxin Reductase Inhibition of a Series of Gold(I) Complexes Containing Hydrophilic Phosphine Ligands. *ChemMedChem* **2010**, *5* (1), 96−102.

(62) Milacic, V.; Chen, D.; Ronconi, L.; Landis-Piwowar, K. R.; Fregona, D.; Dou, Q. P. A Novel Anticancer Gold(III) Dithiocarbamate Compound Inhibits the Activity of a Purified 20S Proteasome and 26S Proteasome in Human Breast Cancer Cell Cultures and Xenografts. *Cancer Res.* **2006**, *66* (21), 10478−10486.

(63) Milacic, V.; Dou, Q. P. The tumor proteasome as a novel target for gold(III) complexes: Implications for breast cancer therapy. *Coord. Chem. Rev.* **2009**, *253* (11), 1649−1660.

(64) Soave, C. L.; Guerin, T.; Liu, J.; Dou, Q. P. Targeting the ubiquitin-proteasome system for cancer treatment: discovering novel inhibitors from nature and drug repurposing. *Cancer Metastasis Rev.* **2017**, *36* (4), 717−736.

(65) Bohan, P. T.; Toste, F. D. Well-Defined Chiral Gold(III) Complex Catalyzed Direct Enantioconvergent Kinetic Resolution of 1,5-Enynes. *J. Am. Chem. Soc.* **2017**, *139* (32), 11016−11019.

(66) Rodriguez, J.; Bourissou, D. Well-Defined Chiral Gold(III) Complexes: New Opportunities in Asymmetric Catalysis. *Angew. Chem., Int. Ed.* **2018**, *57* (2), 386−388.

(67) Messori, L.; Cinellu, M. A.; Merlino, A. Protein Recognition of Gold-Based Drugs: 3D Structure of the Complex Formed When Lysozyme Reacts with Aubipyc. *ACS Med. Chem. Lett.* **2014**, *5* (10), 1110−1113.

(68) Rubbiani, R.; Schuh, E.; Meyer, A.; Lemke, J.; Wimberg, J.; Metzler-Nolte, N.; Meyer, F.; Mohr, F.; Ott, I. TrxR inhibition and antiproliferative activities of structurally diverse gold N-heterocyclic carbene complexes. *MedChemComm* **2013**, *4* (6), 942−948.

(69) Hickey, J. L.; Ruhayel, R. A.; Barnard, P. J.; Baker, M. V.; Berners-Price, S. J.; Filipovska, A. Mitochondria-Targeted Chemotherapeutics: The Rational Design of Gold(I) N-Heterocyclic Carbene Complexes That Are Selectively Toxic to Cancer Cells and Target Protein Selenols in Preference to Thiols. *J. Am. Chem. Soc.* **2008**, *130* (38), 12570−12571.

(70) Messori, L.; Scaletti, F.; Massai, L.; Cinellu, M. A.; Russo Krauss, I.; di Martino, G.; Vergara, A.; Paduano, L.; Merlino, A. Interactions of gold-based drugs with proteins: crystal structure of the adduct formed between ribonuclease A and a cytotoxic gold(iii) compound. *Metallomics* **2014**, *6* (2), 233−236.

(71) Maiore, L.; Cinellu, M. A.; Nobili, S.; Landini, I.; Mini, E.; Gabbiani, C.; Messori, L. Gold(III) complexes with 2-substituted pyridines as experimental anticancer agents: Solution behavior, reactions with model proteins, antiproliferative properties. *J. Inorg. Biochem.* **2012**, *108*, 123−127.

(72) Bhabak, K. P.; Bhuyan, B. J.; Mugesh, G. Bioinorganic and medicinal chemistry: aspects of gold(i)-protein complexes. *Dalton Trans.* **2011**, *40* (10), 2099−2111.

(73) Spell, S. R.; Farrell, N. P. [Au(dien)(N-heterocycle)]3+: Reactivity with Biomolecules and Zinc Finger Peptides. *Inorg. Inorg. Chem.* **2015**, *54* (1), 79−86.

(74) Meister, A. Glutathione metabolism and its selective modification. *J. Biol. Chem.* **1988**, *263* (33), 17205−8.

(75) Williams, M. R. M.; Bertrand, B.; Hughes, D. L.; Waller, Z. A. E.; Schmidt, C.; Ott, I.; O'Connell, M.; Searcey, M.; Bochmann, M. Cyclometallated Au(iii) dithiocarbamate complexes: synthesis, anticancer evaluation and mechanistic studies. *Metallomics* **2018**, *10* (11), 1655−1666.

(76) Boscutti, G.; Marchiò, L.; Ronconi, L.; Fregona, D. Insights into the Reactivity of Gold−Dithiocarbamato Anticancer Agents toward Model Biomolecules by Using Multinuclear NMR Spectroscopy. *Chem. - Eur. J.* **2013**, *19* (40), 13428−13436.

(77) Suntharalingam, K.; Johnstone, T. C.; Bruno, P. M.; Lin, W.; Hemann, M. T.; Lippard, S. J. Bidentate Ligands on Osmium(VI) Nitrido Complexes Control Intracellular Targeting and Cell Death Pathways. *J. Am. Chem. Soc.* **2013**, *135* (38), 14060−14063.

(78) Knopf, K. M.; Murphy, B. L.; MacMillan, S. N.; Baskin, J. M.; Barr, M. P.; Boros, E.; Wilson, J. J. In Vitro Anticancer Activity and in Vivo Biodistribution of Rhenium(I) Tricarbonyl Aqua Complexes. *J. Am. Chem. Soc.* **2017**, *139* (40), 14302−14314.

(79) Saggioro, D.; Rigobello, M. P.; Paloschi, L.; Folda, A.; Moggach, S. A.; Parsons, S.; Ronconi, L.; Fregona, D.; Bindoli, A. Gold(III)-Dithiocarbamato Complexes Induce Cancer Cell Death Triggered by Thioredox System Inhibition and Activation of ERK Pathway. *Chem. Biol.* **2007**, *14* (10), 1128−1139.

(80) Bratsch, S. G. Standard Electrode Potentials and Temperature Coefficients in Water at 298.15 K. *J. Phys. Chem. Ref. Data* **1989**, *18*, 1.

(81) Cinellu, M. A.; Minghetti, G.; Pinna, M. V.; Stoccoro, S.; Zucca, A.; Manassero, M. Synthesis and Characterization of Mononuclear Amidogold(III) Complexes − Crystal Structure of [Au(N2C10H7-(CMe2C6H4)-6)(NHC6H3Me2−2,6)][PF6] − Oxidation of 4-Methylaniline to Azotoluene. *Eur. J. Inorg. Chem.* **2003**, *2003* (12), 2304−2310.

(82) Parkin, S.; Hope, H. Macromolecular Cryocrystallography: Cooling, Mounting, Storage and Transportation of Crystals. *J. Appl. Crystallogr.* **1998**, *31* (6), 945−953.

(83) Hope, H. X-ray Crystallography - A Fast, First-Resort Analytical Tool. *Prog. Inorg. Chem.* **2007**, *41*, 1−19.

(84) *APEX2 Bruker-AXS*; Bruker: Madison, WI, USA, 2006.

(85) Krause, L.; Herbst-Irmer, R.; Sheldrick, G. M.; Stalke, D. Comparison of silver and molybdenum microfocus X-ray sources for single-crystal structure determination. *J. Appl. Crystallogr.* **2015**, *48* (1), 3−10.

(86) Sheldrick, G. M. *SADABS, Program for Bruker Area Detector Absorption Correction*; University of Gottingen: Gottingen, 1997.

(87) Sheldrick, G. M. Crystal structure refinement with SHELXL. *Acta Crystallogr. C Struct. Chem.* **2015**, *71* (1), 3−8.

(88) Sheldrick, G. M. SHELXT - integrated space-group and crystal-structure determination. *Acta Crystallogr. A Found Adv.* **2015**, *71* (1), 3−8.

(89) Sheldrick, G. A short history of SHELX. *Acta Crystallogr., Sect. A: Found. Crystallogr.* **2008**, *64* (1), 112−122.

(90) Spek, A. L. Structure validation in chemical crystallography. *Acta Crystallogr. D Biol. Crystallogr.* **2009**, *65* (2), 148−155.

(91) Parkin, S. Expansion of scalar validation criteria to three dimensions: the R tensor. *Acta Crystallogr. A* **2000**, *56*, 157−162.